iScience

CellPress
OPEN ACCESS

Article

Horizontal mtDNA transfer between cells is common during mouse development

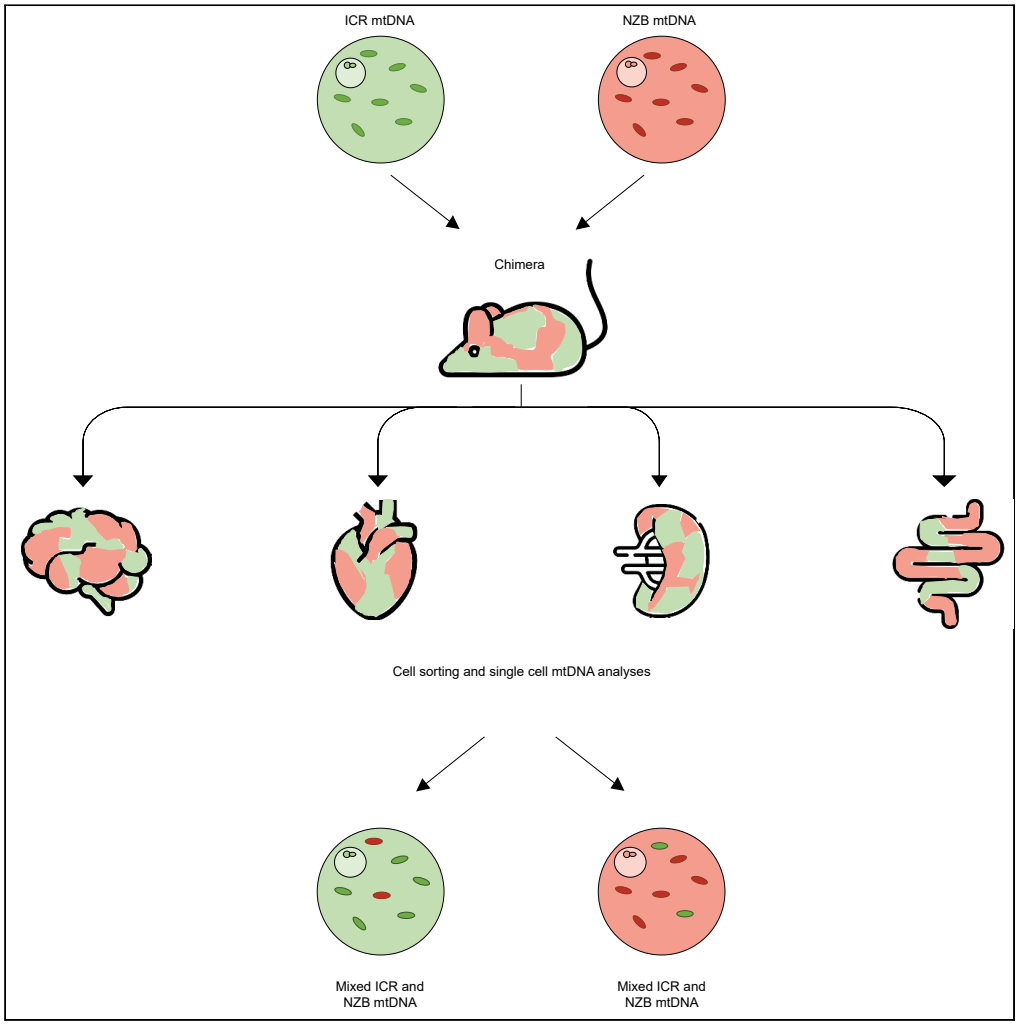

Nuria Marti Gutierrez, Aleksei Mikhalchenko, Hong Ma, ..., Anthony Paul Barnes, Paula Amato, Shoukhrat Mitalipov

shoukhrat@gmail.com

Highlights

Individual cells in adult mouse chimeras acquire donor mtDNA horizontally

Significant percentage of cardiomyocytes, neurons, and glia were heteroplasmic

Donor mtDNA heteroplasmy in these cells can reach up to 50%

Pathogenic mtDNA mutations may potentiate horizontal acquisition of wild-type mtDNA

Marti Gutierrez et al., iScience *25*, 103901
March 18, 2022
https://doi.org/10.1016/j.isci.2022.103901

iScience

CellPress
OPEN ACCESS

Article

Horizontal mtDNA transfer between cells is common during mouse development

Nuria Marti Gutierrez,[1,6] Aleksei Mikhalchenko,[1,6] Hong Ma,[1] Amy Koski,[1] Ying Li,[1] Crystal Van Dyken,[1] Rebecca Tippner-Hedges,[1] David Yoon,[1] Dan Liang,[1] Tomonari Hayama,[1] David Battaglia,[1] Eunju Kang,[2,5] Yeonmi Lee,[2,5] Anthony Paul Barnes,[3] Paula Amato,[1,4] and Shoukhrat Mitalipov[1,7,*]

SUMMARY

Cells transmit their genomes vertically to daughter cells during cell divisions. Here, we demonstrate the occurrence and extent of horizontal mitochondrial (mt)DNA acquisition between cells that are not in a parent-offspring relationship. Extensive single-cell sequencing from various tissues and organs of adult chimeric mice composed of cells carrying distinct mtDNA haplotypes showed that a substantial fraction of individual cardiomyocytes, neurons, glia, intestinal, and spleen cells captured donor mtDNA at high levels. In addition, chimeras composed of cells with wild-type and mutant mtDNA exhibited increased trafficking of wild-type mtDNA to mutant cells, suggesting that horizontal mtDNA transfer may be a compensatory mechanism to restore compromised mitochondrial function. These findings establish the groundwork for further investigations to identify mtDNA donor cells and mechanisms of transfer that could be critical to the development of novel gene therapies.

INTRODUCTION

Mitochondria are essential cytoplasmic organelles that contain their own genome (mtDNA) encoding 37 genes, including critical OXPHOS proteins, rRNAs, and tRNAs (Dyall et al., 2004; Wallace, 1994). mtDNA is markedly different from nuclear DNA, with nearly exclusive maternal *trans*-generational inheritance (from the oocyte) and the existence of thousands of mtDNA copies per cell. Mutations in oocyte mtDNA cause maternally inherited syndromes in children (Schon et al., 2012; Stewart and Chinnery, 2015; Wallace, 2018), whereas somatic mtDNA mutations are implicated in the etiology of many age-related conditions including neurodegenerative diseases, cancer, and diabetes (López-Otín et al., 2013; Nunnari and Suomalainen, 2012; Schapira, 2012).

It is known that mammalian cells transmit both nuclear and mitochondrial genomes vertically to daughter cells during cell divisions. However, recent studies have demonstrated horizontal transmission of mitochondria and mtDNA between cells that are not in a parent-offspring relationship. Such horizontal mitochondrial trafficking appears to be common between some cell lines co-cultured *in vitro* (Spees et al., 2006; Sun et al., 2019). However, the strongest genetic evidence comes from the phylogenetic studies of canine sexually transmissible venereal tumors originated approximately 11,000 years ago. Interestingly, analysis of mtDNA suggested that cancer cells periodically acquired novel mtDNA from their hosts, possibly to rescue cancer cells from accumulated deleterious mtDNA mutations (Rebbeck et al., 2011). Grafting of murine breast carcinoma or metastatic melanoma cells depleted of mtDNA into syngeneic host mice resulted in restoration of respiration due to acquisition of donor mtDNA from host tissues (Tan et al., 2015). Although these studies show horizontal acquisition of mtDNA in pathological conditions such as cancer, we reasoned that intercellular mtDNA trafficking could as well be a fundamental physiological process during normal development with an important role in maintaining metabolic potential of cells, particularly in postmitotic tissues with limited renewal from stem cell pools.

This assumption is supported by several lines of evidence demonstrating horizontal trafficking of mitochondria as organelles. For example, astrocytes were shown to provide metabolic support to adjacent neurons by donating healthy mitochondria, thus ensuring neuronal recovery (Davis et al., 2014), whereas neurons were shown to transfer damaged mitochondria to astrocytes for disposal and recycling (Hayakawa et al.,

[1]Center for Embryonic Cell and Gene Therapy, Oregon Health & Science University, Portland, OR 97239, USA

[2]Stem Cell Center & Department of Convergence Medicine, Asan Medical Center, University of Ulsan College of Medicine, Seoul 05505, South Korea

[3]Knight Cardiovascular Institute, Department of Medicine, Oregon Health & Science University, Portland, OR 97239, USA

[4]Department of Obstetrics and Gynecology, Oregon Health & Science University, Portland, OR 97239, USA

[5]Present address: Center for Embryo and Stem Cell Research, CHA Advanced Research Institute, CHA University, Seongnam, Gyeonggi, 13488, South Korea.

[6]These authors contributed equally

[7]Lead contact

*Correspondence: shoukhrat@gmail.com

https://doi.org/10.1016/j.isci.2022.103901

2016). In addition, endothelial progenitor cells may transfer their mitochondria to support brain endothelial cell energetics, barrier integrity, and angiogenic function (Hayakawa et al., 2018). Importantly, the majority of horizontal mitochondrial movement observations are based on either fluorescence microscopy or recovery of metabolic function but lack genetic evidence of donor mtDNA acquisition. Sequencing-based detection of donor mtDNA transfer in a typical mammalian organism is not feasible because all cells contain identical mtDNA. To overcome this barrier, we generated mouse chimeras consisting of cells from two distinct mouse strains carrying divergent mtDNA haplotypes. This model allowed us to trace horizontal transmission of mtDNA in various organs and tissues through single-cell sequencing. Here we demonstrate clear evidence of horizontal mtDNA acquisition in tissues with high energy demand such as heart and brain. Our results also revealed that intercellular mtDNA acquisition is not limited to postmitotic cells but is also common in tissues with greater self-renewal capacity. Furthermore, our observations suggest that horizontal mtDNA acquisition can increase in response to mitochondrial respiration compromise due to mtDNA damage, implying its role as a compensatory mechanism to restore normal metabolic activity.

RESULTS

Generating a chimera model to study horizontal mtDNA transmission

We generated intermitochondrial mouse chimeras consisting of two cell lineages carrying divergent mtDNA haplotypes to create conditions for tractable horizontal mtDNA acquisition via DNA sequencing. We also confirmed that the mitochondrial genomes of NZB/J (NZB) and ICR strains differ at 88 single nucleotide variants (SNVs) using whole mtDNA sequencing (Figure S1A; Table S1). These SNVs were dispersed throughout the genome, including within protein coding genes (n = 68, including 15 amino acids changes), tRNA (n = 3), rRNA (n = 7), and noncoding control region (n = 10).

Our initial attempt to generate chimeras by aggregating 4-cell embryos from ICR and NZB mice do not produce chimeric offspring, likely due to poor development of NZB embryos. We overcame this limitation by establishing one male and four female karyotypically normal ESC lines from 33 NZB blastocysts. One female cell line was transduced to stably express a Td-Tomato reporter gene under the control of the Ubiquitin-C promoter (Shibuya et al., 2003; Yamaguchi et al., 2012). This genetically tagged cell line was injected into host ICR 4-cell embryos followed by blastocyst transfer into pseudopregnant recipient mice (Figures S1B and S1C). Based on coat color pigmentation, 46 of the total 107 live offspring (43%) were identified as chimeras (Figure S1C). We subjected DNA from ear biopsies of coat color chimeras for qPCR analysis to confirm chimerism based on the presence of Td-Tomato DNA. This assay revealed the contribution of NZB/ESC progeny ranging from 0.5% to 83.6% in all 46 mice (Table S2). Based on these results, chimeras were grouped into low ($\leq$ 15% of NZB/ESC contribution) and high chimerism (> 15%; Figure S1D). To determine the degree of chimerism in various organs and tissues, adult chimeras were euthanized and NZB contribution was measured in bulk DNA isolated from heart, brain, intestine, spleen, kidney, liver, testis, cumulus cells, and oocytes. NZB contribution in these tissues ranged from 4.3%–64.3% in spleen, 4.6%–66.6% in brain, 2.6%–54.5% in heart, and 1.9%–46.3% in intestine. However, kidney (0%–28.6%) and liver (0%–7.9%) tissues carried relatively lower NZB contribution (Figure S1E, Table 1).

Testicular and cumulus cells were also chimeric with NZB contribution ranging from 3%–33.3% in testis and 36.1%–52.6% in cumulus cells. However, none of the individual mature oocytes genotyped were NZB (Figure S1E, Table 1). Nevertheless, we paired 14 female chimeras with ICR males but all 155 offspring were albino (ICR). Genetic analysis confirmed that all offspring were ICR, suggesting a lack of ESC germline transmission (Figure S1F).

Detection of mtDNA heteroplasmy in individual cardiomyocytes

To test out hypothesis that horizontal mtDNA acquisition might occur in postmitotic tissues, we initially analyzed individual cardiomyocytes of chimera Ch9, which exhibited a high contribution of NZB/ESCs in heart (45.2%). Heart muscle was dissociated into individual cardiomyocytes and characterized by the expression of cardiac troponin T (Figure S2A). Because of large cell size, FAC sorting for NZB and ICR cells was not successful. DNA from 35 individual cardiomyocytes was isolated and analyzed for mtDNA heteroplasmy by three independent sequencing assays (Sanger, ARMS-qPCR and WGS; Figure S1A). To avoid contamination with cell-free mtDNA, each cardiomyocyte was extensively rinsed in several drops of medium before mtDNA isolation. Sanger sequencing examined heteroplasmy based on four SNVs differentiating NZB and ICR mtDNA and revealed that 15 out of a total of 35 (42.9%) cardiomyocytes from the Ch9 chimera exhibited both NZB and ICR haplotypes (Figures 1A and 1B). Next, the same cardiomyocytes

Table 1. Contribution of NZB/ESCs and B6/ESCs to organs and tissues

Chimera ID	Age	Gender	Ear (%)	Spleen (%)	Brain (%)	Heart (%)	Intestine (%)	Kidney (%)	Liver (%)	Testis (%)	Cumulus Cells (%)	Oocytes (%)
Ch-1	2 m	Male	4.6	4.3	5.2	4.8	2.1	0	0	3	N/A	N/A
Ch-2	21 m	Female	8.5	18	6	8	5.4	2.1	0	N/A	N/A	N/A
Ch-3	8 m	Male	16.1	16	6.2	3.6	2.7	6	5.1	12	N/A	N/A
Ch-4	18 m	Male	17.8	18.8	4.6	18	24.2	3.3	0	8.7	N/A	N/A
Ch-5	6 m	Male	25.3	13.1	8.4	11.8	1.9	0	0	14.6	N/A	N/A
Ch-6	19 m	Male	30	5.1	37.4	16.3	10	3.5	0.1	20.4	N/A	N/A
Ch-7	5 m	Male	30.5	5.4	22	18.2	6	0	2	4.1	N/A	N/A
Ch-8	15 m	Male	35.1	30.4	66.6	34.5	24.1	15.1	2	22.4	N/A	N/A
Ch-9	4 m	Male	40.1	34.9	33.4	45.2	40.3	1.7	0.2	30.3	N/A	N/A
Ch-10	5 m	Female	42.4	47.5	35.9	26.5	37.4	18.5	5.7	N/A	36.1	0
Ch-11	13 m	Female	43.2	64.3	36.3	24.1	36.2	11	3	N/A	48.7	0
Ch-12	17 m	Male	52	6	20.6	26.7	26.7	15	0.5	N/A	N/A	N/A
Ch-13	12 m	Male	57.2	53.4	31.7	2.6	17.1	9.8	4	16	N/A	N/A
Ch-14	13 m	Female	67.7	42	34.6	18.3	9.7	28.6	7.9	N/A	52.6	0
Ch-15	13 m	Male	68	47.6	34.9	21.3	6.8	3.7	3.6	7.4	N/A	N/A
Ch-16	6 m	Female	76.5	15.9	33.1	47.7	26.2	20.4	2.7	N/A	46.1	0
Ch-17	17 m	Male	83.6	5.1	11.3	54.5	46.3	20	0.8	33.3	N/A	N/A
Average			41.1	25.2	25.2	22.5	19	9.3	2.2	15.7	45.9	0
MutCh-1	21 m	Female	19.2	16.1	39.3	40.7	38.9	N/T	N/T	N/T	N/T	N/T
MutCh-2	21 m	Male	30.1	7.3	33.6	18.1	14.6	N/T	N/T	N/T	N/T	N/T
MutCh-3	17 m	Male	32.3	51.9	59.3	75.8	70	N/T	N/T	N/T	N/T	N/T
MutCh-4	12 m	Male	42.1	33.1	38.5	47.7	61.4	N/T	N/T	N/T	N/T	N/T
MutCh-5	19 m	Male	43.7	32.3	60.8	56.6	12	N/T	N/T	N/T	N/T	N/T
MutCh-6	13 m	Male	51.7	14.7	40.4	40.8	68.4	N/T	N/T	N/T	N/T	N/T
MutCh-7	12 m	Male	61.3	50	94	88	69.4	N/T	N/T	N/T	N/T	N/T
Average			40.1	29.3	52.3	52.5	47.8					

were analyzed by ARMS-qPCR to determine the relative contribution of NZB and ICR mtDNA in heteroplasmic cardiomyocytes. Because the nuclear genetic origin of cardiomyocytes was unknown, we assigned the major mtDNA haplotype to maternal, whereas the minor haplotype was considered as acquired donor mtDNA. Among 35 analyzed cardiomyocytes, 20 appeared homoplasmic (3 NZB and 17 ICR), whereas 15 cells revealed heteroplasmy (Figure 1B) with minor, donor mtDNA contribution ranging from 4.4 to 44.9% (mean donor mtDNA 20.3% and median 15.9%; Figure 1C). To eliminate the possibility that detected heteroplasmy was caused by *de novo* mutations or sequencing errors, we corroborated Sanger and qPCR results by whole mtDNA sequencing (WGS), which allowed simultaneous interrogation of all 88 SNVs, discriminating NZB and ICR haplotypes. Due to low mtDNA yield, only nine heteroplasmic and one homoplasmic cardiomyocyte samples were sequenced by WGS. Results confirmed the presence of both NZB and ICR mtDNA variants in all nine individual cardiomyocytes, clearly demonstrating that these cardiomyocytes were indeed heteroplasmic (Figure 1D). The average heteroplasmy for donor mtDNA was measured at 16.2%, ranging from 1.5% to 39.1% (Figure 1D, Table S3).

To ensure that heteroplasmy found in individual cardiomyocytes in chimeric mice is not due to contamination or sequencing errors, several controls were included. Individual cardiomyocytes from nonchimeric ICR and NZB mice were analyzed using Sanger sequencing and all were homoplasmic for the expected haplotype (n = 35 ICR and n = 28 NZB cardiomyocytes). Additional controls were employed to eliminate the possibility of contamination with cell-free mtDNA by premixing chopped heart tissues from control nonchimeric ICR and NZB mice and then collecting individual cells. A total of 177 individual control cardiomyocytes from six different premixed experiments were collected and only 11 (6.2%) cardiomyocytes showed mtDNA heteroplasmy by Sanger sequencing (Figure 1E). We also measured heteroplasmy levels in these

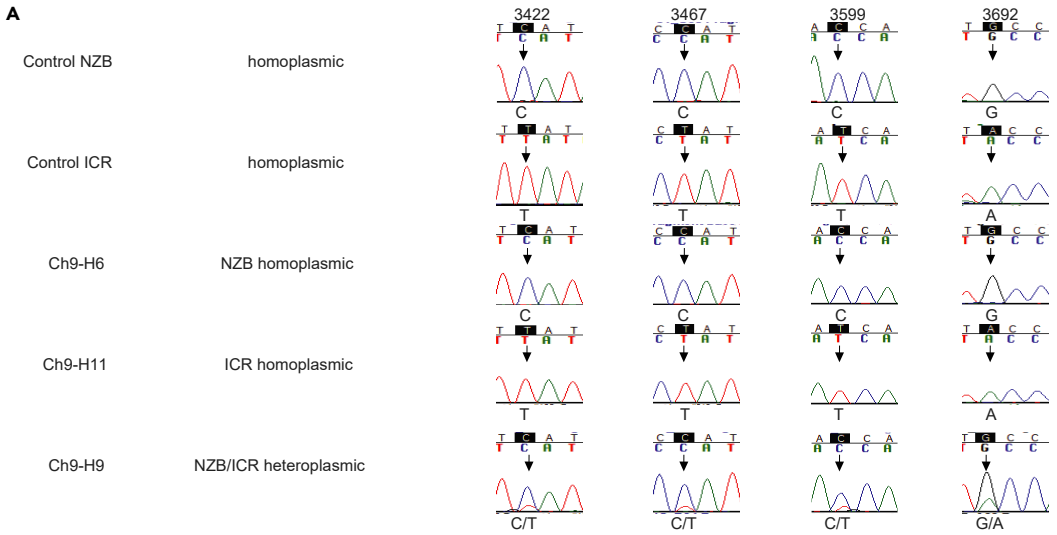
A
3422
3467
3599
3692
Control NZB
homoplasmic
C
C
C
G
Control ICR
homoplasmic
T
T
A
Ch9-H6
NZB homoplasmic
C
C
C
G
Ch9-H11
ICR homoplasmic
T
T
T
A
Ch9-H9
NZB/ICR heteroplasmic
C/T
C/T
C/T
G/A

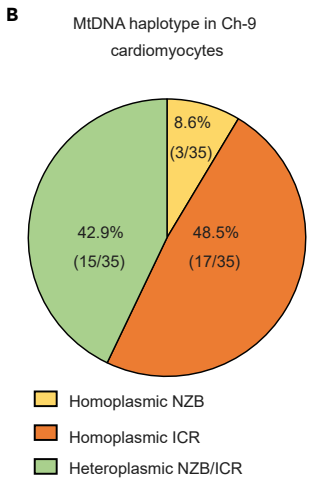
B
MtDNA haplotype in Ch-9
cardiomyocytes
8.6%
(3/35)
42.9%
(15/35)
48.5%
(17/35)
Homoplasmic NZB
Homoplasmic ICR
Heteroplasmic NZB/ICR

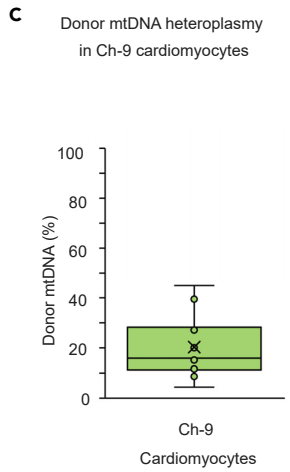
C
Donor mtDNA heteroplasmy
in Ch-9 cardiomyocytes
Donor mtDNA (%)
100
80
60
40
20
0
Ch-9
Cardiomyocytes

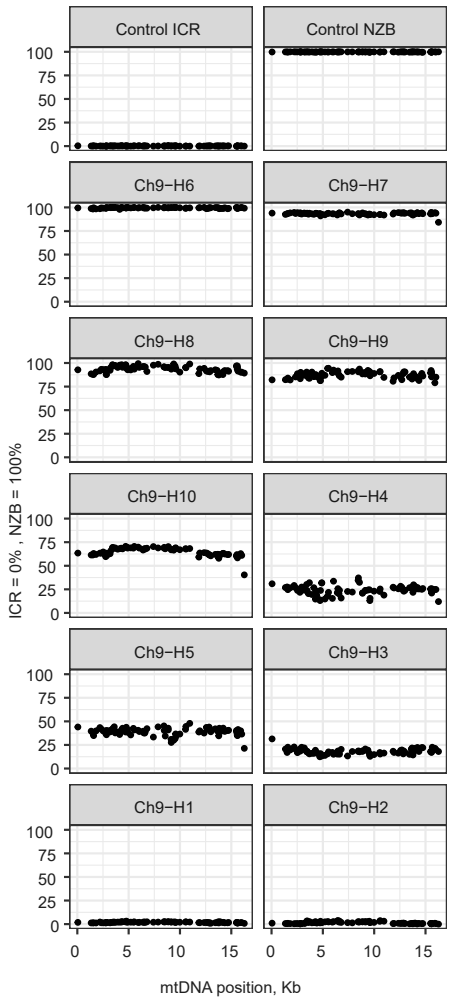
D
Whole mtDNA sequencing (88 SNVs)
Control ICR
Control NZB
Ch9−H6
Ch9−H7
Ch9−H8
Ch9−H9
Ch9−H10
Ch9−H4
Ch9−H5
Ch9−H3
Ch9−H1
Ch9−H2
ICR = 0% , NZB = 100%
100
75
50
25
0
0
5
10
15
mtDNA position, Kb

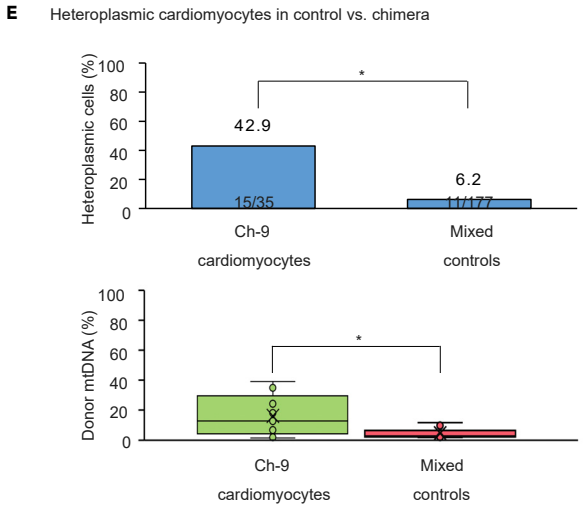
E
Heteroplasmic cardiomyocytes in control vs. chimera
Heteroplasmic cells (%)
100
80
60
40
20
0
*
42.9
15/35
6.2
11/177
Ch-9
cardiomyocytes
Mixed
controls
Donor mtDNA (%)
100
80
60
40
20
0
*
Ch-9
cardiomyocytes
Mixed
controls

Figure 1. mtDNA heteroplasmy in individual cardiomyocytes in ICR/NZB chimeric heart

(A) Sanger sequencing of individual cardiomyocytes to detect mtDNA SNVs specific for ICR and NZB haplotypes.

(B) Summary of mtDNA haplotypes in individual cardiomyocytes from the chimera Ch9.

(C) Heteroplasmy for donor mtDNA in cardiomyocytes measured by ARMS-qPCR. Horizontal line inside the box represents median and x represents mean.

(D) Heteroplasmy measured by whole mtDNA sequencing that surveys simultaneously 88 SNVs in control and Ch9 cardiomyocytes. Each data point represents one unique site; 0% indicates ICR strain and 100% indicates NZB strain.

(E) Frequency of heteroplasmic cells found in individual cardiomyocytes of Ch9 and mixed control mice and their heteroplasmy levels. * indicates significant ($p < 0.05$) differences among groups. Fisher exact test with two tails was used for the comparison between frequency of heteroplasmic cardiomyocytes. Student's t test was used for comparison of heteroplasmy level.

control cardiomyocytes by WGS. Although these observations suggest some possibility of contamination with cell-free mtDNA, the percentage of heteroplasmic cardiomyocytes found in chimeras was significantly higher than controls (42.9% versus 6.2% $p < 0.05$). Moreover, heteroplasmy levels in cardiomyocytes from chimeras were also higher than controls (16.2% versus 4.6% $p < 0.05$) (Figure 1E). Therefore, it is reasonable to conclude that the mtDNA heteroplasmy present in most individual cardiomyocytes in chimeras is likely due to horizontal mtDNA acquisition.

To determine if horizontal mtDNA acquisition in cardiomyocytes is a common phenomenon, we next analyzed hearts from an additional 16 chimeric mice. The results confirmed that 12 of 17 chimeras contained heteroplasmic cardiomyocytes (Figure 2A). Single-cell mtDNA analyses carried out by three independent sequencing approaches as described earlier revealed that 86/293 individual cardiomyocytes collected from these 12 chimeras were heteroplasmic, containing two mtDNA haplotypes (Figure 2B). The proportion of heteroplasmic cardiomyocytes in these mice ranged from 4.8% to 54.8% (Figure 2C). Heteroplasmy levels measured by ARMS-qPCR for the minor (donor) mtDNA haplotype ranged from 2% to 45.5%, with an average of 19.1% and median of 15.2% (Figures 2D and 2E). We corroborated these results by WGS in 61 cardiomyocytes. An average heteroplasmy level for donor mtDNA was measured at 19.1%, with median of 18% and ranging from 1.5% to 49.3% (Table S3). Assuming that the maternal mtDNA is the major component in heteroplasmic cardiomyocytes, a similar percentage of ICR (28.5%; 55/193) and NZB (31%; 31/100) cardiomyocytes acquired donor mtDNA. Interestingly, mean donor mtDNA heteroplasmy level appeared significantly higher in NZB cells (26.4%) compared with that in ICR cardiomyocytes (16.5% $p < 0.05$; Figure 2F). This may be explained by the fact that in most chimeras NZB/ESCs contribution in heart tissue was lower than ICR. Therefore, NZB cardiomyocytes were surrounded by more ICR cells, and thus had more opportunity to acquire donor ICR mtDNA. Lack of heteroplasmic cardiomyocytes in the remaining five chimeras may be explained by a very low NZB contribution (6.1%) that led to a small sample size of collected NZB cells (8/134) (Figure 2G).

Overall, the frequency of heteroplasmy (29.4% versus 6.2%) and heteroplasmy levels (19.1% versus 4.6%; Table S4) found in cardiomyocytes from chimeras were significantly higher than in control nonchimeric hearts, suggesting identified heteroplasmy is due to horizontal mtDNA gains (Figure 2H).

In summary, our results indicate that a substantial portion of analyzed individual cardiomyocytes in chimeric animals are heteroplasmic, containing a mixture of NZB and ICR mtDNA haplotypes. High heteroplasmy levels for both haplotypes in these cardiomyocytes suggest horizontal mtDNA transmission. However, we cannot completely exclude the possibility that some heteroplasmy is due to contamination during tissue and single-cell preparations.

mtDNA heteroplasmy in neurons and glia

We expanded our horizontal mtDNA studies to the brain, another organ that possess limited self-renewal. Whole adult brains were dissociated and purified as single-cell suspensions that based on cell-type markers contained neurons (NeuN), oligodendrocytes (Olig2), microglia (Iba1), and astrocytes (Sox9). The majority of labeled cells were positive for oligodendrocyte markers (50.6%), whereas the remaining cells were astrocytes (26%), neurons (16.4%), and microglia (0.5%) (Figure S2B).

In contrast to cardiomyocytes, dissociated cells from the brain were smaller, which allowed FAC sorting to separate cells positive for Td-tomato (NZB) from ICR cells (Figure S2C). Single-cell suspensions from 13 chimeric mouse brains were sorted, repeatedly rinsed in multiple drops of medium, and individual cells were collected for mtDNA analyses. Controls and sham medium from the last rinsed drop were also collected and analyzed for the presence of cell-free mtDNA.

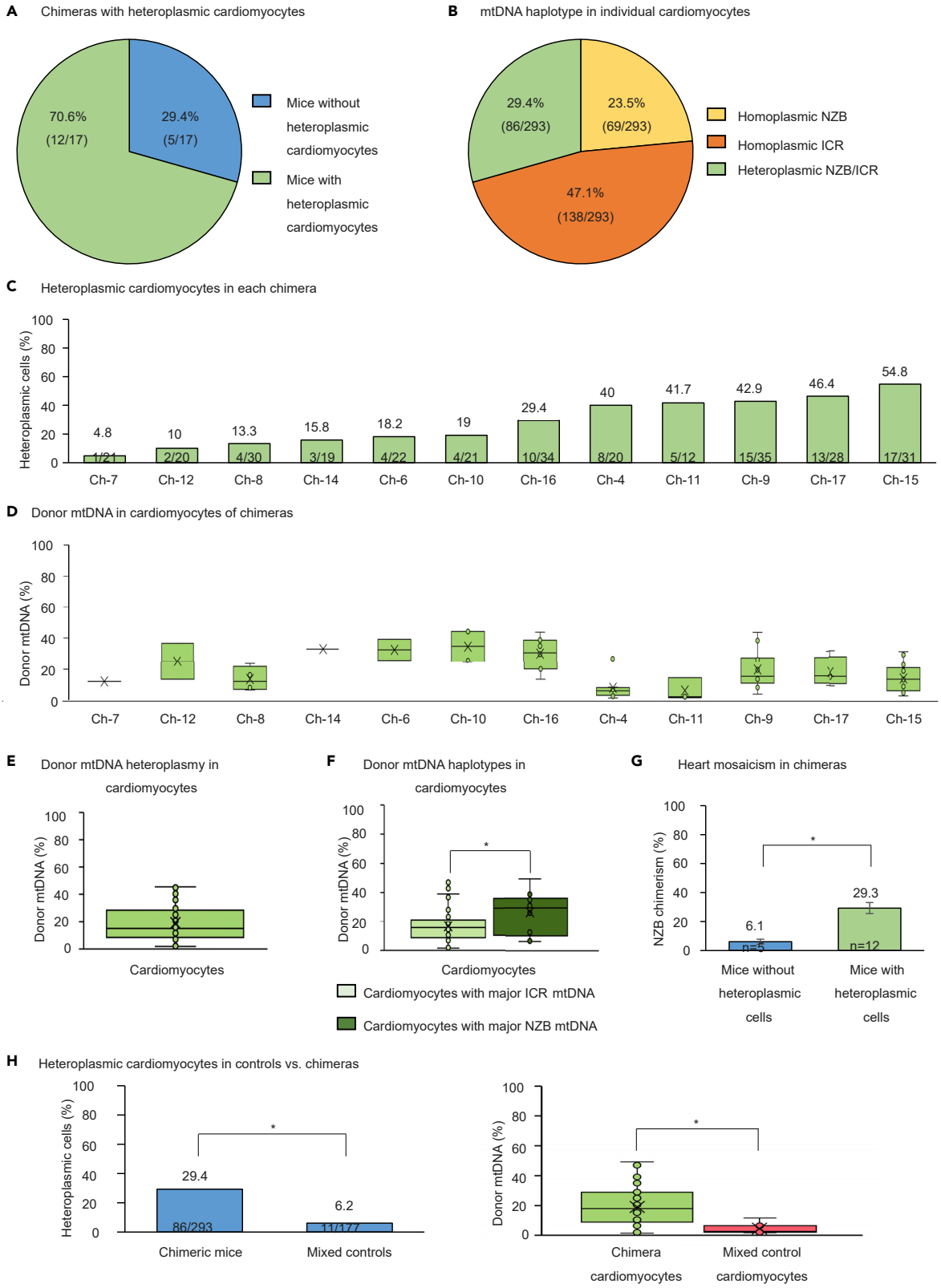
A
Chimeras with heteroplasmic cardiomyocytes
70.6%
(12/17)
29.4%
(5/17)
Mice without heteroplasmic cardiomyocytes
Mice with heteroplasmic cardiomyocytes
B
mtDNA haplotype in individual cardiomyocytes
29.4%
(86/293)
23.5%
(69/293)
47.1%
(138/293)
Homoplasmic NZB
Homoplasmic ICR
Heteroplasmic NZB/ICR
C
Heteroplasmic cardiomyocytes in each chimera
Heteroplasmic cells (%)
4.8
1/21
10
2/20
13.3
4/30
15.8
3/19
18.2
4/22
19
4/21
29.4
10/34
40
8/20
41.7
5/12
42.9
15/35
46.4
13/28
54.8
17/31
Ch-7
Ch-12
Ch-8
Ch-14
Ch-6
Ch-10
Ch-16
Ch-4
Ch-11
Ch-9
Ch-17
Ch-15
D
Donor mtDNA in cardiomyocytes of chimeras
Donor mtDNA (%)
E
Donor mtDNA heteroplasmy in cardiomyocytes
Donor mtDNA (%)
Cardiomyocytes
F
Donor mtDNA haplotypes in cardiomyocytes
Donor mtDNA (%)
*
Cardiomyocytes
Cardiomyocytes with major ICR mtDNA
Cardiomyocytes with major NZB mtDNA
G
Heart mosaicism in chimeras
NZB chimerism (%)
*
6.1
n=5
29.3
n=12
Mice without heteroplasmic cells
Mice with heteroplasmic cells
H
Heteroplasmic cardiomyocytes in controls vs. chimeras
Heteroplasmic cells (%)
*
29.4
86/293
6.2
11/177
Chimeric mice
Mixed controls
Donor mtDNA (%)
*
Chimera cardiomyocytes
Mixed control cardiomyocytes

Figure 2. mtDNA heteroplasmy in individual cardiomyocytes of chimeras

(A) Proportion of chimeras with and without donor mtDNA in cardiomyocytes.

(B) Summary of mtDNA haplotypes seen in individual cardiomyocytes of chimeras.

(C) Proportion of heteroplasmic cardiomyocytes in each tested chimeric mouse.

(D) Mean and median donor mtDNA heteroplasmy levels in heteroplasmic cardiomyocytes of each chimera measured by ARMS-qPCR. Horizontal lines inside the boxes represent median and x represent mean.

(E) Average donor mtDNA heteroplasmy levels in all heteroplasmic cardiomyocytes. Horizontal line inside the box shows the median value, and x indicates mean.

(F) Cardiomyocytes with donor (minor) mtDNA heteroplasmy levels for each ICR and NZB mtDNA haplotype. * indicates significant ($p < 0.05$) differences among groups. Student's t test was used for comparison of heteroplasmy level.

(G) ESC (NZB) contribution to hearts in chimeras with and without donor mtDNA in cardiomyocytes. * indicates significant ($p < 0.05$) differences between groups. N shows number of mice in each group. Student's t test was used for comparison of chimerism level.

(H) Number of heteroplasmic cells and mean heteroplasmy levels in individual cardiomyocytes of chimeras and mixed controls. * indicates significant ($p < 0.05$) differences among groups. Fisher exact test with two tails was used for the comparison between frequency of heteroplasmic cardiomyocytes. Student's t test was used for comparison of heteroplasmy level.

Independent analyses of mtDNA revealed that 10 out of 13 total chimeric brains examined contained heteroplasmic neurons (Figure 3A). Sanger sequencing of individual brain cells from 10 chimeras revealed that approximately half (46.5%; 73/157) were heteroplasmic containing a mixture of ICR and NZB haplotypes (Figure 3B). The percentage of heteroplasmic cells in the NZB fraction (14/23, 60.9%) was higher than in the ICR group (59/134, 44%) (Figure 3C). To validate Sanger results, heteroplasmic brain cells were also examined by WGS as described earlier. Analysis of 88 informative SNVs showed that all cells were indeed heteroplasmic containing a mixture of two different mtDNA haplotypes (Figure 3D). The average heteroplasmy level for donor NZB mtDNA in individual ICR cells was 22.1% ranging from 4.4% to 44.1%. Meanwhile, the average heteroplasmy for donor ICR mtDNA in individual NZB cells was 34.8% (Figure 3E and Table S3).

In the three chimeras negative for heteroplasmic cells, contribution of NZB cells to brain tissue was significantly lower (5.8%) than in mice with heteroplasmic brain cells (31.1%) (Figure 3F). Moreover, FAC sorting of brain cells from low chimeras failed to produce NZB cells; all cells collected and analyzed were from the ICR fraction and all were homoplasmic for ICR mtDNA haplotype. Cells collected from control, nonchimeric ICR or NZB brain did not reveal any heteroplasmy. We detected low heteroplasmy in a few controls (6/61 cells; 9.8%) collected from premixed ICR and NZB brain cells from six control experiments, indicating contamination with cell-free mtDNA. However, the percentage of heteroplasmic cells and their heteroplasmy levels in controls were significantly lower than that in chimeras (9.8% versus 46.5% and 6.9% versus 24%, respectively) (Figure 3G and Table S4), indicating that most heteroplasmy found in chimeras should be valid and not due to contamination.

In summary, similar to our findings in cardiomyocytes, a large proportion of analyzed individual cells isolated from the brains of chimeric mice carried a mixture of both ICR and NZB mtDNA haplotypes. This indicates that cells within the brain also acquire donor mtDNA horizontally from cells with a different mtDNA lineage in the absence of injury or pathology. This finding would indicate that horizontal transfer represents a facet of normal physiology in these largely postmitotic tissues.

Horizontal mtDNA transfer in mitotically active tissues

We also examined a set of organs that contain a high proportion of mitotically active cells that included the intestine, spleen, liver, and kidney. Initially, mtDNA from individual intestinal cells derived from 14 chimeric mice were sorted for Td-tomato (Figure S2C) and analyzed by Sanger sequencing for heteroplasmy at four informative SNVs. Heteroplasmic cells were detected in eight chimeras, whereas cells from the remaining six animals were all homoplasmic (Figure 4A). From chimeras with heteroplasmic cells, a total of 178 individual intestinal cells, including 96 of NZB and 82 of ICR origin, were sequenced. From this set of cells, 23 (12.9%, 13 NZB and 10 ICR) showed a mixture of both mtDNA haplotypes (Figure 4B). Although three animals had low contribution of the NZB genotype (2.1%–10%). Interestingly, only NZB cells in these chimeras were heteroplasmic, whereas all examined ICR cells were homoplasmic. In the other five chimeras with high NZB contribution (17.1%–46.3%), both NZB and ICR cells showed heteroplasmy (Figure 4C).

Among the six chimeras without any heteroplasmic intestinal cells, four animals exhibited low NZB contribution in intestinal tissues (1.9%–6.8%). We failed to recover any intestinal cells from the NZB fraction after sorting in these mice but collected and sequenced 67 ICR cells. The remaining two mice showed higher

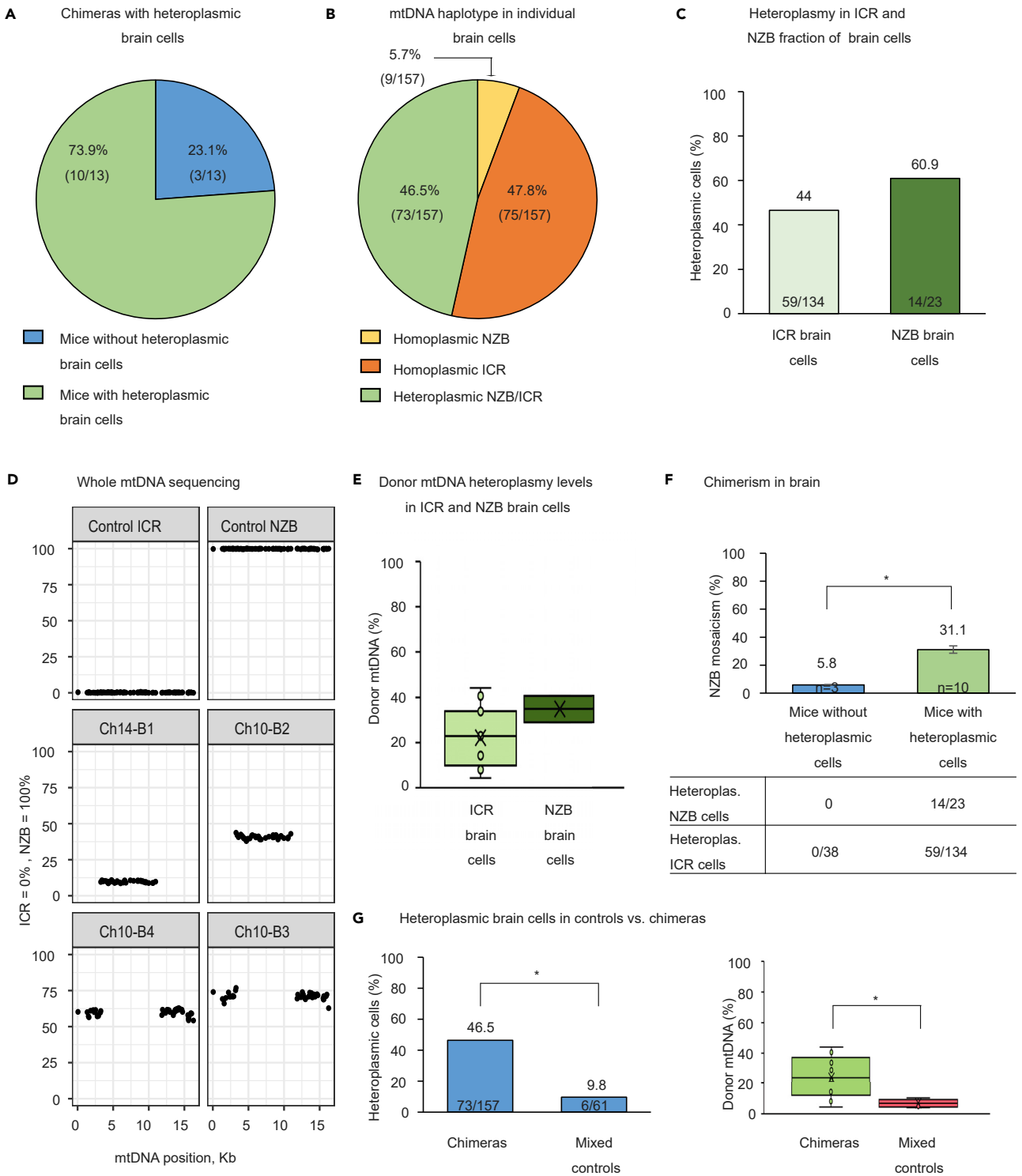

	Mice without heteroplasmic cells	Mice with heteroplasmic cells
Heteroplas. NZB cells	0	14/23
Heteroplas. ICR cells	0/38	59/134

Figure 3. mtDNA heteroplasmy in individual brain cells from ICR/NZB chimeras

(A) Number of chimeras with and without heteroplasmic brain cells.

(B) Summary mtDNA haplotypes in individual brain cells.

(C) Number of heteroplasmic brain cells in ICR and NZB fractions.

(D) Whole mtDNA sequencing in brain cells from controls and chimeras. Each data point represents one unique site; 0% indicates ICR strain and 100% indicates NZB strain.

Figure 3. *Continued*

(E) Mean donor mtDNA heteroplasmy levels in individual brain cells from ICR and NZB fractions. Horizontal line inside the box indicates median, and x indicates mean value.

(F) Differences in ESC (NZB) contribution to cerebrum chimeras with and without heteroplasmic brain cells. * indicates significant ($p < 0.05$) differences between groups. N shows number of mice in each group. Student's t test was used for comparison of chimerism level.

(G) Number of heteroplasmic cells and mean heteroplasmy levels in individual brain cells in ICR/NZB chimeras and mixed controls. * indicates significant ($p < 0.05$) differences between groups. Fisher exact test with two tails was used for the comparison between frequency of heteroplasmic brain cells. Student's t test was used for comparison of heteroplasmy level.

chimerism, and both NZB (N = 18) and ICR (N = 6) cells were collected but all were homoplasmic for maternal mtDNA haplotype (Figure S2D).

A total of 283 individual spleen cells recovered from the same 14 chimeras were also sorted and processed for mtDNA sequencing. Among those, heteroplasmic cells were detected in five chimeras with high NZB contribution (18–64.3%; Figures 4D and 4E). In these animals, 27 out of 160 (16.9%) sequenced cells carried mixed mtDNA from both haplotypes (Figure 4F). In the remaining nine animals, all tested spleen cells (N = 123) were homoplasmic for corresponding NZB or ICR mtDNA haplotypes (Figure S2E).

In control, nonchimeric ICR and NZB animals, individual intestinal and spleen cells were homoplasmic as expected. However, 3/109 intestinal cells (2.8%) from 6 premixed control mice showed a small amount of heteroplasmy, indicating contamination with cell-free mtDNA. Similarly, 3/84 premixed control spleen cells from six animals were heteroplasmic. Importantly, the frequency of heteroplasmic cells in controls was lower than in chimeras (2.8% versus 12.9% in intestine; 3.6% versus 16.9% in spleen) (Figures 4G and 4H, Table S4). These data suggest that most mtDNA heteroplasmy found in chimeras is a result of horizontal mtDNA acquisition.

Sanger sequencing results were validated with WGS and confirmed heteroplasmy in intestinal and spleen cells is indeed a result of coexistence of both ICR and NZB haplotypes (Table S3) and heteroplasmy levels in heteroplasmic control cells were lower than in chimeras (7.6% versus 39.1% in intestine; 6.4% versus 19.7% in spleen) (Figures 4G and 4H, Table S4). We next collected and analyzed 218 individual liver and 263 kidney cells from 13 chimeric mice. Of these, 12 liver and 7 kidney cells were heteroplasmic (Figure S2F). In premixed controls 2/43 liver and 1/82 kidney cells were also heteroplasmic (Table S4).

In summary, our results suggest that similar to cardiac and brain cells, intestinal, spleen, liver, and kidney cells may also acquire donor mtDNA horizontally.

Age-related changes in donor mtDNA acquisition

We reasoned that horizontal mtDNA transmission could be a cellular mechanism compensating for age-related metabolic decline and investigated whether intercellular mtDNA acquisition is affected by the age of chimeric mice. Among 17 chimeras examined earlier, five were young ($\leq$ 6 months of age), whereas 10 mice were old ($\geq$ 12 months), and one mouse was 8 months old (Table 1).

We compared mtDNA heteroplasmy results in heart, brain, intestinal, and spleen cells between young and aged chimeras. The analyses did not reveal significant differences in the proportion of heteroplasmic cells found in most tissues (heart: 27% in young versus 30.8% in aged; brain: 56.1% in young versus 41% in aged; intestine: 19% in young versus 10% in aged; Figure 5A). In spleen, heteroplasmic cells were detected only in aged chimeras but not in younger mice; however, this could be due to low chimerism in spleen of young chimeras (Figure 5A). We further analyzed heteroplasmy levels as a function of age in heart, brain, and intestine where we had heteroplasmy measurements in both groups but did not find any significant differences (Figure 5B). In summary, although heteroplasmy levels in most organs did not change with age, donor mtDNA acquisition in spleen cells was seen only in aged animals.

Horizontal mtDNA transfer increased after mtDNA damage

Another possible factor that might affect horizontal mtDNA exchange is a compromised metabolic function caused by pathogenic mtDNA mutations. To investigate this hypothesis, we generated an ESC line carrying defective mtDNA using PolG mutator mice and B6 UBC-GFP mice as recently described (Ma et al., 2020). These ESCs were on wild-type C57Bl6/J (B6) background tagged with GFP but carrying a homoplasmic mtDNA mutation (5082A > C) affecting tRNA-Ala with homology to human MELAS such as encephalopathy. Cells exhibited compromised mitochondrial respiratory function due to reduced activity of

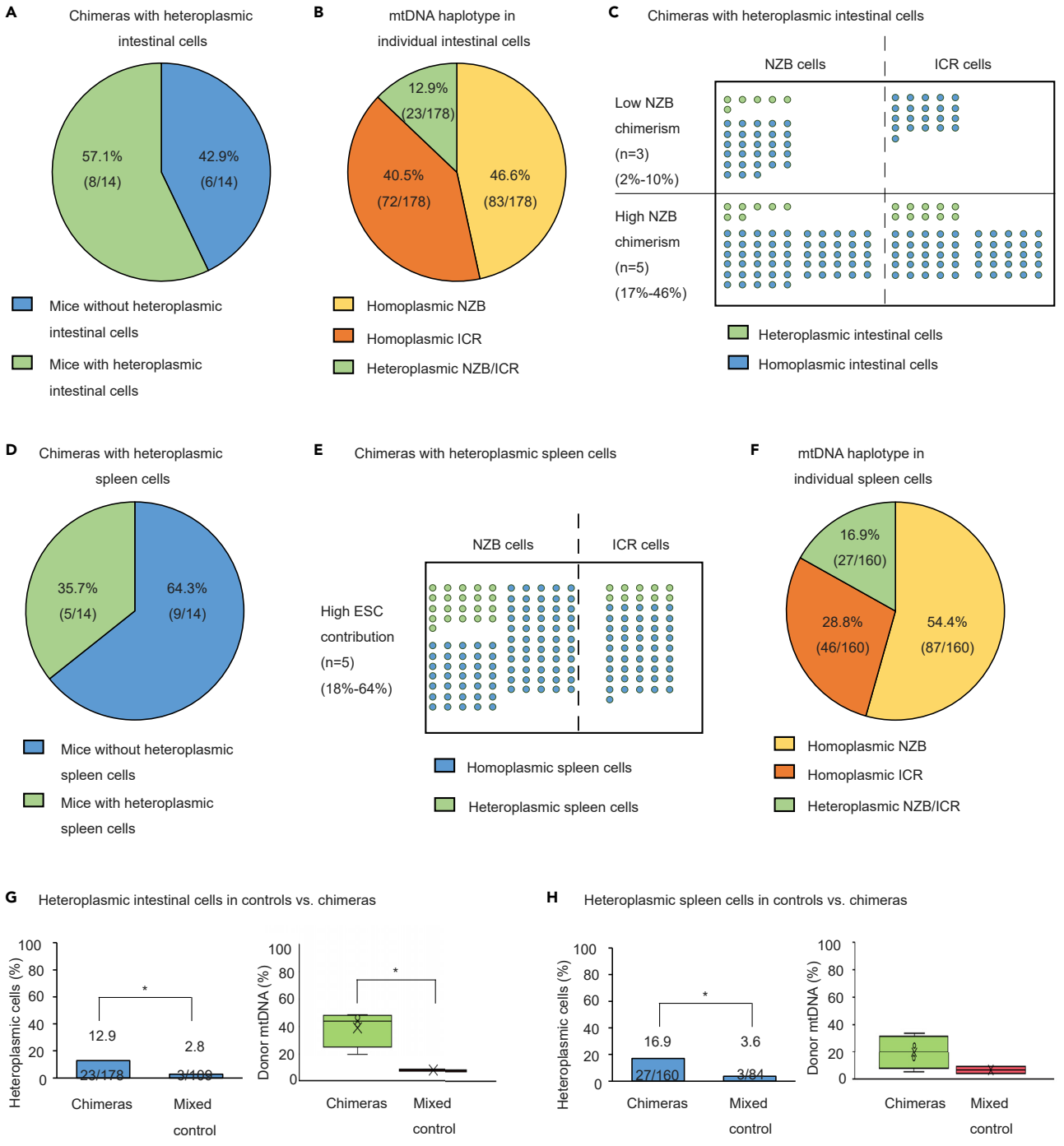

Figure 4. mtDNA heteroplasmy in individual intestinal and spleen cells

(A) Number of chimeras with and without heteroplasmic intestinal cells.

(B) Summary of mtDNA haplotypes in individual intestinal cells.

(C) Degree of ESC (NZB) contribution affects heteroplasmy for donor mtDNA. Each dot represents individual intestinal cell. Green dots represent heteroplasmic and blue dots indicate homoplasmic intestinal cells. Chimeras with low and high ESC contribution show donor mtDNA in intestinal cells from NZB fraction. Only chimeras with high ESC contribution show ICR intestinal cells with donor mtDNA. All intestinal cells of ICR fraction from chimeras with low ESC contribution appeared homoplasmic.

(D) Number of chimeras with and without heteroplasmic spleen cells.

(E) Chimeras with high ESC contribution revealed cells with donor mtDNA in both ICR and NZB fractions. Each dot represents individual spleen cell. Green dots indicate heteroplasmic spleen cells, and blue dots depict homoplasmic spleen cells.

(F) Summary of mtDNA haplotypes in individual spleen cells.

Figure 4. *Continued*

(G) Number and heteroplasmy levels in individual intestinal cells from ICR/NZB chimeras and mixed controls. * indicates significant ($p < 0.05$) differences between groups. Fisher exact test with two tails was used for the comparison between frequency of heteroplasmic intestinal cells. Student's t test was used for comparison of heteroplasmy level.

(H) Number and heteroplasmy levels in individual spleen cells from ICR/NZB chimeras and mixed controls. * indicates significant ($p < 0.05$) differences between groups. Fisher exact test with two tails was used for the comparison between frequency of heteroplasmic spleen cells. Student's t test was used for comparison of heteroplasmy level.

mitochondrial complex I (Table S5). ESCs were injected into 662 host NZB embryos and transferred into recipients (Figure 5C). NZB and B6 mtDNA differ in 89 SNVs, but both strains have black fur, precluding chimerism determination by coat color. We therefore examined 32 offspring by sequencing for the presence of the B6-specific genomic variant and identified 16 chimeric pups (7 females and nine males) (Figure 5C and Table S2). We next divided offspring into groups with low ($\leq$ 15% of ESC contribution; n = 7) and high chimerism ($\geq$ 15%; n = 9) (Figure 5D).

We also evaluated female germline transmission of B6 ESCs by pairing three female chimeras with ICR males. All 30 pups examined showed NZB nDNA, suggesting a lack of germline transmission of the B6 genotype.

All high chimeras (6 males and 1 female) were euthanized between 12 and 21 months of age, and chimerism in heart, brain, intestine, and spleen organs was further confirmed by ARMS-qPCR (Table 1). Next, tissues were dissociated into single cells and FAC sorted based on GFP expression (Figure S2C) to separate B6 and NZB fractions, with exception of cardiomyocytes. In spleen and intestinal cells, the proportion of heteroplasmic cells was not significantly different between B6 and NZB fractions. However, in cardiomyocytes (with B6 mtDNA as the major component) and in brain cells, the number of heteroplasmic B6 cells was significantly higher than in NZB fraction (Figure 5E). Specifically, 15.9% of B6 cardiomyocytes carried donor NZB mtDNA and only 1.7% of NZB cells acquired donor B6 mtDNA. In brain, 64.5% of B6 cell received donor mtDNA, whereas 37.5% of NZB cells acquired B6 mtDNA (Figure 5E). Further heteroplasmy levels in cardiomyocytes and brain cells were analyzed by WGS. The average heteroplasmy levels in B6 cardiomyocytes was 29.7% (12.5%–41.2%) compared with 25.6% in the NZB fraction (Figure 5F; Table S3). In B6 brain cells, the average heteroplasmy level for donor mtDNA was at 31.2% versus 23.4% in NZB cells (Figure 5F; Table S3).

These results suggest that intercellular mtDNA transfer may play a role in maintaining the metabolic potential of cells with dysfunctional mutant mtDNA.

Horizontal mtDNA transmission in reproductive tissues

Although germline transmission of female ES cells was not observed in our chimeras, we assessed whether donor mtDNA could still be acquired by oocytes from the somatic compartment of ovaries and follicles. All 155 pups born from NZB/ICR chimeras were albino (ICR). Analysis of nuclear DNA in ear biopsies via qPCR did not reveal the presence of Td-Tomato sequence associated with the NZB strain, indicating that all offspring were of ICR origin (Figure S1F). WGS for mtDNA revealed that all pups were homoplasmic for the ICR haplotype with no traces of donor NZB mtDNA. Similarly, all 30 pups born from the B6/NZB chimeras were of NZB genotype, and mtDNA sequencing did not detect any heteroplasmy with the donor B6 haplotype.

We also examined 81 mature MII oocytes and individual cumulus cells from NZB/ICR chimeras. A total of 62 individual cumulus cells had their mtDNA analyzed via Sanger sequencing, and all were homoplasmic for NZB (N = 25) or ICR (N = 37) haplotypes, suggesting chimerism in follicular cells surrounding oocytes (Figure S2G). However, all oocytes were of ICR origin and WGS of their mtDNA did not detect any heteroplasmy with the donor NZB haplotype (Figures S2G and S2H; Table S3).

In addition, we analyzed testicular cells from nine male NZB/ICR chimeras. The samples were chimeric, with a contribution of NZB/ESCs progeny ranging from 3% to 33.3% (average of 15.7%; Table 1 and Figure S1E). We analyzed mtDNA by sequencing 142 individual cells isolated from testicles and 19 were homoplasmic for NZB mtDNA, whereas the remaining 123 were homoplasmic for ICR mtDNA (Figure S2G). We also validated Sanger results with WGS in four testicular cells and six cumulus cells and confirmed that all were homoplasmic (Figure S2H; Table S3).

These results indicate that despite chimerism in the somatic cell compartment, oocytes, and offspring of female chimeras were all homoplasmic.

A Cells with donor mtDNA in young and aged chimeras

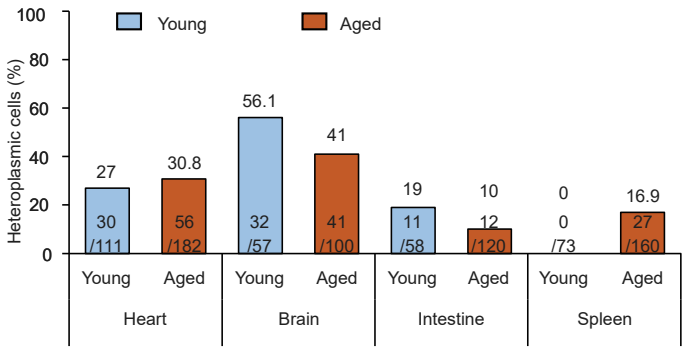

B Donor mtDNA heteroplasmy in young and aged chimeras

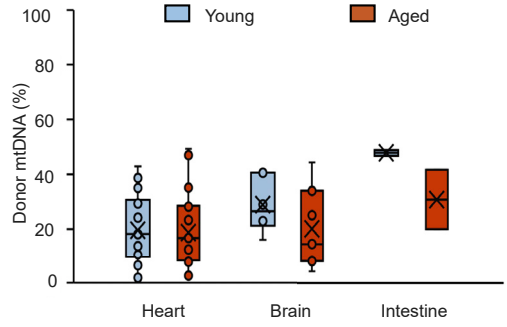

C Full term development of chimeric NZB wt-mtDNA/B6 mut-mtDNA embryos

N, embryos transferred (ET)	N, recipient mice (RM)	N, pregnant recipients (%)	N, recipients delivered offspring (%)	N, full term offspring (% per ET)	N, Live offspring (% per ET)	N, chimeric offspring (% per live offspring)
662	46	31 (67%)	15 (33%)	36 (5.4%)	32 (4.8%)	16 (50%)

D Contribution of B6/ESCs in chimeras

Group	N, mice	Sex	B6/ESC contribution	Median
Low chimerism (0.1%-15%)	6	Female	2.9%-13%	5%
	1	Male	14.1%	14.1%
High chimerism (15%-99%)	1	Female	19.2%	19.2%
	8	Male	30.1%-68.2%	42.9%

E Donor mtDNA in wt and mutant chimeras

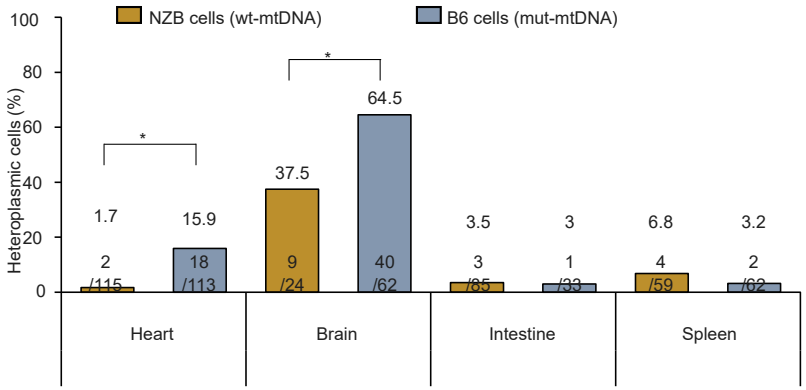

F Donor mtDNA heteroplasmy in wt and mutant cells in chimeras

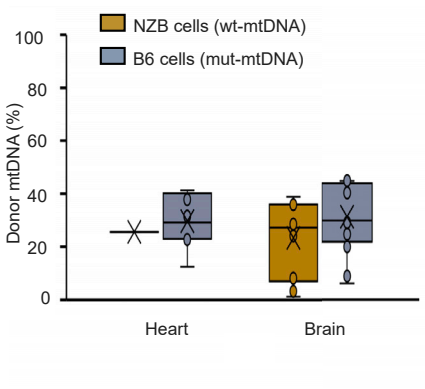

Figure 5. Changes in horizontal mtDNA acquisition during aging and in mice with mtDNA mutation

(A) Proportion of heteroplasmic cells in heart, brain, intestine, and spleen in young and aged chimeras. Young chimeras did not show donor mtDNA in spleen cells.

(B) Mean and median donor mtDNA heteroplasmy levels in young and aged chimeras. Horizontal line inside the boxes indicates median and x indicates mean values.

(C) Full-term development of chimeric embryos with mtDNA mutation. Pregnancy was estimated based on implantation sites in the recipient uterus.

(D) Contribution of B6/ESC with mutants mtDNA to chimeras.

Figure 5. *Continued*

(E) Number of individual B6 and NZB heart, brain, intestinal, and spleen cells that acquired donor mtDNA. * indicates significant ($p < 0.05$) differences among groups. Fisher exact test with two tails was used for the comparison between frequency of heteroplasmic cells.

(F) Heteroplasmy for donor mtDNA in NZB and B6 (mutant) cardiomyocytes and brain cells. Horizontal line inside the boxes depicts median, and x shows mean values

DISCUSSION

Horizontal mitochondrial gene transfer is a relatively common phenomenon in plants that is facilitated during direct contact between host and parasite plant species and, perhaps, after grafting (Bergthorsson et al., 2003; Davis and Wurdack, 2004; Mower et al., 2004; Stegemann and Bock, 2009). However, in regard to animals, current dogma holds that cells transmit both their nuclear and mitochondrial genomes exclusively to daughter cells (vertically) during cell division. The only exception was found in interorganismal transmissible tumors when engrafted cancer cells acquired donor mtDNA from host tissues (Rebbeck et al., 2011). Several recent studies observed horizontal transfer of cellular organelles including mitochondria using imaging-based assays or based on recovery of metabolic function of recipient cells (Davis et al., 2014; Hayakawa et al., 2016, 2018; Islam et al., 2012; Tan et al., 2015). However, direct genetic evidence for horizontal mtDNA transfer between normal cells during development and aging of mammalian organisms is lacking.

Detection of horizontal mtDNA transmission using genetic tracing within a normal organ or organism is extremely problematic because all cells will contain identical mtDNA. Here we generated chimeric mice composed of cells from two divergent strains carrying genetically distinct mtDNA haplotypes. Other key requirements for detection of donor mtDNA in chimeric organs and tissues are separation of two cell populations and evaluating heteroplasmy at the single cell level. This prerequisite, although extremely time and labor consuming, is critical to eliminate contaminations and false-positive outcomes.

Our unique experimental approach provides strong evidence displaying a widespread intercellular mtDNA acquisition in various mouse organs. The results shown here suggest horizontal mtDNA transfer may be a common process that is likely required to maintain the metabolic capacity of cells, particularly in postmitotic tissues with limited or absent stem cell pools. However, due to the complexity of the single cell isolation and collection from chimeras we cannot rule out the possibility that some detected heteroplasmy is due to cross contamination. We found high heteroplasmy in cells collected from metabolically active tissues including heart and brain (Chow et al., 2017; Lane, 2011). It is believed that cardiomyocytes and neurons have greater vulnerability to mtDNA damage due to high metabolic demands and lack of self-renewal capacity, leading to progressive age-related decline in mitochondrial function (Lane, 2011; Wallace, 2005). Not surprisingly, cardiovascular and neurodegenerative diseases rank as leading causes of death, both in the United States and globally (Kochanek et al., 2020).

Increased donor mtDNA acquisition in chimeras composed of cells carrying normal and mutant mtDNA was also shown. This mutation is associated with compromised mitochondrial respiratory function, and increased acquisition of normal mtDNA by mutant cells in chimeras implies that horizontal mtDNA transfer could be a compensatory mechanism required to restore mitochondrial function. We recently demonstrated that most pathogenic mtDNA mutations are lethal in normal nonchimeric mice but can be rescued in chimeras (Ma et al., 2020). Here, we show a likely mechanism by which chimeric mice carrying cells with mutant and wild-type mtDNA can avoid clinical manifestation of disease and live a normal lifespan.

As we recently demonstrated, in contrast to humans, somatic mtDNA mutations are not prevalent in most organs and tissues during mouse aging (Ma et al., 2018). Because an increase in donor mtDNA acquisition depends on mtDNA damage, these findings might explain our observation that heteroplasmy levels in most organs in young and old chimeras did not change. However, in contrast to young animals, older chimeras exhibited heteroplasmy in spleen.

The presence of donor mtDNA in most cells was detected at high levels, suggesting that horizontal mitochondrial transport can significantly affect metabolic function. The average heteroplasmy level for donor mtDNA in cardiomyocytes, brain, intestinal, and spleen cells was 21.1%. However, it is likely that each cell in a chimeric organism also receives mitochondria from cells of the same strain containing identical mtDNA. Therefore, it is likely that cells acquire more donor mtDNA than we were able to detect.

We have previously shown that horizontal mitochondrial transfer can be achieved microsurgically in monkey and human mature oocytes (Tachibana, 2009, 2013). This technique, termed mitochondrial

replacement therapy (MRT), involves nearly complete removal of cytoplasm containing mutant maternal mtDNA in a patient oocyte and replacing it with donor cytoplasm and mtDNA from the healthy oocyte (Kang et al., 2016). Such MRT oocytes, after fertilization and transfer into recipients, develop into live offspring containing donor mtDNA and age normally without negative consequences (Ma et al., 2021). MRT has been successfully used in humans to prevent transmission of maternally inherited mtDNA disease to children (Zhang, 2017). This proof-of-concept approach demonstrates that gene therapy for mtDNA disease can be accomplished by horizontal mtDNA transfer. Obviously, microsurgical MRT procedures developed for oocytes are not applicable for patient somatic cells *in vivo* residing in enormous numbers in organs and tissues. Novel somatic cell MRT approaches, however, can be developed based on physiological mechanisms of horizontal mtDNA acquisition discovered in our study.

Future investigations of horizontal mtDNA transfer are required to facilitate the development of an effective somatic gene therapy for mitochondrial diseases. It is critical to uncover which cell types are donors of mtDNA and the exact mechanism by which cells transmit and accept mtDNA horizontally.

Our chimeric mice contain a mixture of two cell populations in most or all organs, thus allowing to survey the acquisition of donor mtDNA by recipient cells. However, the limiting factor of this model is that the mtDNA donor cells remain unknown. It is not clear if donor mtDNA in cardiomyocytes and brain tissue originate from the same cell types in a tissue or are provided by other cells from different tissues such as hematopoietic or glial cells. Further, it is also plausible that tissue-specific stem cells including mesenchymal stromal cells or hematopoietic stem cells are mitochondrial donors in some tissues or organs. Additional animal models, with single organ or tissue transplantation, are required to determine the exact mtDNA donor and recipient cells for each tissue.

Although our data clearly indicate that horizontal mtDNA acquisition occurs in cells of various organs in mice, we cannot rule out low heteroplasmy levels in some cells may be caused by false-positive detection of cell-free mtDNA. Similarly, true heteroplasmy may be masked in cells that appear homoplasmic due to false-negative results when donor mtDNA is originated from cells of the same strain as mtDNA recipient.

The molecular and signaling mechanisms by which cells donate and acquire mitochondria and mtDNA horizontally remain poorly understood. Several mechanisms have been proposed, including tunneling nanotubes (TNTs) (Rustom et al., 2004), extracellular vesicles, gap junctions, exocytosis and endocytosis of naked mitochondria, and whole cell fusion (Qin et al., 2021). Cell fusion in cardiomyocytes (Ali et al., 2020; Matsuura et al., 2004; Qin et al., 2021) and neurons (Giordano-Santini et al., 2016) has been documented and could explain heteroplasmy in chimeras. It is possible that different somatic cells and tissues utilize varied mechanisms of horizontal mtDNA transfer.

We hope that our study will facilitate future investigations to address the basic biology of this phenomenon and develop future gene therapies based on horizontal mtDNA transfer that would allow delivery and replacement of mtDNA in tissues and organs impacted by mitochondrial diseases.

Limitations of the study

The experimental design of this study is based on mtDNA analysis of individual cells isolated from chimeric organs and tissues of adult mice. As shown in our control treatments, technical limitations and difficulties in single-cell isolation can produce false-positive heteroplasmy readouts due to extracellular mtDNA contamination. Although critical for detection of heteroplasmic cells, our chimera approach is not suitable for identification the mtDNA donor cells.

STAR★METHODS

Detailed methods are provided in the online version of this paper and include the following:

- KEY RESOURCES TABLE
- RESOURCE AVAILABILITY
  - Lead contact
  - Materials availability
  - Data and code availability
- EXPERIMENTAL MODEL AND SUBJECT DETAILS
  - Mice strains

SUPPLEMENTAL INFORMATION

Supplemental information can be found online at https://doi.org/10.1016/j.isci.2022.103901.

ACKNOWLEDGMENTS

The authors acknowledge the OHSU Institutional Animal Care and Use Committee (IACUC) and Department of Comparative Medicine (DCM) for providing animal care, oversight, and guidance. We thank OHSU Vollum Institute, OHSU Flow Cytometry Core, and Molecular Technologies Core at ONPRC for their services and support. We are indebted to Hayley Darby, Riffat Ahmed, Thanasup Gonmanee, and Yibing Jia for their expertise and services. Studies were supported by the grants from the National Institutes of Health (NIH) (RO1AG062459), the Burroughs Wellcome Fund, the Collins Medical trust, National Research Foundation of Korea (NRF-2018R1A2B3001244), Asan Medical Center (2019-755), and OHSU institutional funds.

AUTHOR CONTRIBUTIONS

N.M.G., A.M., P.A., and S.M. conceived the study and designed the experiments. C.V.D. managed mice colony. N.M.G. generated chimera embryos. D.L., T.H., C.V.D., and Y.L. performed embryo transfers. N.M.G., A.M., H.M., D.Y., D.L., T.H., and D.B. performed tissue collection, disaggregation into single cells, and single cells collection. N.M.G., A.M., D.Y., Y.L., C.V.D., R.T.H., A.K., D.L., and H.M. prepared samples for Sanger sequencing and performed qPCR. Y.L., E.K., and Y.Lee prepared mtDNA and performed MiSeq assays. N.M.G., A.M., and H.M performed NGS data analysis and interpretation. A.B. performed immunostaining. N.M.G., A.M., P.A., and S.M. analyzed data and wrote the paper.

DECLARATION OF INTEREST

The authors declare no competing interest.

Received: November 29, 2021
Revised: January 12, 2022
Accepted: February 7, 2022
Published: March 18, 2022

REFERENCES

Ali, S.R., Menendez-Montes, I., Warshaw, J., Xiao, F., and Sadek, H.A. (2020). Homotypic fusion generates multinucleated cardiomyocytes in the murine heart. Circulation *141*, 1940–1942. https://doi.org/10.1161/circulationaha.119.043530.

Bergthorsson, U., Adams, K.L., Thomason, B., and Palmer, J.D. (2003). Widespread horizontal transfer of mitochondrial genes in flowering plants. Nature *424*, 197–201. https://doi.org/10.1038/nature01743.

Chow, J., Rahman, J., Achermann, J.C., Dattani, M.T., and Rahman, S. (2017). Mitochondrial disease and endocrine dysfunction. Nat. Rev. Endocrinol. *13*, 92–104. https://doi.org/10.1038/nrendo.2016.151.

Davis, C.C., and Wurdack, K.J. (2004). Host-to-parasite gene transfer in flowering plants: phylogenetic evidence from malpighiales. Science *305*, 676–678. https://doi.org/10.1126/science.1100671.

Davis, C.H., Kim, K.Y., Bushong, E.A., Mills, E.A., Boassa, D., Shih, T., Kinebuchi, M., Phan, S., Zhou, Y., Bihlmeyer, N.A., et al. (2014). Transcellular degradation of axonal mitochondria. Proc. Natl. Acad. Sci. U S A. *111*, 9633–9638. https://doi.org/10.1073/pnas.1404651111.

Dyall, S.D., Brown, M.T., and Johnson, P.J. (2004). Ancient invasions: from endosymbionts to organelles. Science *304*, 253–257. https://doi.org/10.1126/science.1094884.

Giordano-Santini, R., Linton, C., and Hilliard, M.A. (2016). Cell-cell fusion in the nervous system: alternative mechanisms of development, injury, and repair. Semin. Cell Dev Biol *60*, 146–154. https://doi.org/10.1016/j.semcdb.2016.06.019.

Guez-Barber, D., Fanous, S., Harvey, B.K., Zhang, Y., Lehrmann, E., Becker, K.G., Picciotto, M.R., and Hope, B.T. (2012). FACS purification of immunolabeled cell types from adult rat brain. J. Neurosci. Methods *203*, 10–18. https://doi.org/10.1016/j.jneumeth.2011.08.045.

Hayakawa, K., Chan, S.J., Mandeville, E.T., Park, J.H., Bruzzese, M., Montaner, J., Arai, K., Rosell, A., and Lo, E.H. (2018). Protective effects of endothelial progenitor cell-derived extracellular mitochondria in brain endothelium. Stem Cells *36*, 1404–1410.

Hayakawa, K., Esposito, E., Wang, X., Terasaki, Y., Liu, Y., Xing, C., Ji, X., and Lo, E.H. (2016). Transfer of mitochondria from astrocytes to neurons after stroke. Nature *535*, 551–555. https://doi.org/10.1038/nature18928.

Islam, M.N., Das, S.R., Emin, M.T., Wei, M., Sun, L., Westphalen, K., Rowlands, D.J., Quadri, S.K., Bhattacharya, S., and Bhattacharya, J. (2012). Mitochondrial transfer from bone-marrow-derived stromal cells to pulmonary alveoli protects against acute lung injury. Nat. Med. *18*, 759–765. https://doi.org/10.1038/nm.2736.

Kang, E., Wu, J., Gutierrez, N.M., Koski, A., Tippner-Hedges, R., Agaronyan, K., Platero-Luengo, A., Martinez-Redondo, P., Ma, H., Lee, Y., et al. (2016). Mitochondrial replacement in human oocytes carrying pathogenic mitochondrial DNA mutations. Nature *540*, 270–275. https://doi.org/10.1038/nature20592.

Kochanek, K.D., Xu, J., and Arias, E. (2020). Mortality in the United States, 2019 (NCHS Data Brief), pp. 1–8.

Lane, N. (2011). The costs of breathing. Science *334*, 184–185. https://doi.org/10.1126/science.1214012.

Lee, H.S., Ma, H., Juanes, R.C., Tachibana, M., Sparman, M., Woodward, J., Ramsey, C., Xu, J., Kang, E.J., Amato, P., et al. (2012). Rapid mitochondrial DNA segregation in primate preimplantation embryos precedes somatic and germline bottleneck. Cell Rep. *1*, 506–515. https://doi.org/10.1016/j.celrep.2012.03.011.

López-Otín, C., Blasco, M.A., Partridge, L., Serrano, M., and Kroemer, G. (2013). The hallmarks of aging. Cell *153*, 1194–1217. https://doi.org/10.1016/j.cell.2013.05.039.

Ma, H., Hayama, T., Van Dyken, C., Darby, H., Koski, A., Lee, Y., Gutierrez, N.M., Yamada, S., Li, Y., Andrews, M., et al. (2020). Deleterious mtDNA mutations are common in mature oocytes. Biol. Reprod. *102*, 607–619. https://doi.org/10.1093/biolre/ioz202.

Ma, H., Lee, Y., Hayama, T., Van Dyken, C., Marti-Gutierrez, N., Li, Y., Ahmed, R., Koski, A., Kang, E., Darby, H., et al. (2018). Germline and somatic mtDNA mutations in mouse aging. PLoS One *13*, e0201304. https://doi.org/10.1371/journal.pone.0201304.

Ma, H., Van Dyken, C., Darby, H., Mikhalchenko, A., Marti-Gutierrez, N., Koski, A., Liang, D., Li, Y., Tippner-Hedges, R., Kang, E., et al. (2021). Germline transmission of donor, maternal and paternal mtDNA in primates. Hum. Reprod. *36*, 493–505. https://doi.org/10.1093/humrep/deaa308.

Matsuura, K., Wada, H., Nagai, T., Iijima, Y., Minamino, T., Sano, M., Akazawa, H., Molkentin, J.D., Kasanuki, H., and Komuro, I. (2004). Cardiomyocytes fuse with surrounding noncardiomyocytes and reenter the cell cycle. J. Cell Biol *167*, 351–363. https://doi.org/10.1083/jcb.200312111.

Mower, J.P., Stefanović, S., Young, G.J., and Palmer, J.D. (2004). Plant genetics: gene transfer from parasitic to host plants. Nature *432*, 165–166. https://doi.org/10.1038/432165b.

Nunnari, J., and Suomalainen, A. (2012). Mitochondria: in sickness and in health. Cell *148*, 1145–1159. https://doi.org/10.1016/j.cell.2012.02.035.

Qin, Y., Jiang, X., Yang, Q., Zhao, J., Zhou, Q., and Zhou, Y. (2021). The functions, methods, and mobility of mitochondrial transfer between cells. Front Oncol. *11*, 672781. https://doi.org/10.3389/fonc.2021.672781.

Rebbeck, C.A., Leroi, A.M., and Burt, A. (2011). Mitochondrial capture by a transmissible cancer. Science *331*, 303. https://doi.org/10.1126/science.1197696.

Rustom, A., Saffrich, R., Markovic, I., Walther, P., and Gerdes, H.H. (2004). Nanotubular highways for intercellular organelle transport. Science *303*, 1007–1010. https://doi.org/10.1126/science.1093133.

Schapira, A.H. (2012). Mitochondrial diseases. Lancet *379*, 1825–1834. https://doi.org/10.1016/s0140-6736(11)61305-6.

Schon, E.A., DiMauro, S., and Hirano, M. (2012). Human mitochondrial DNA: roles of inherited and somatic mutations. Nat. Rev. Genet. *13*, 878–890. https://doi.org/10.1038/nrg3275.

Shibuya, K., Shirakawa, J., Kameyama, T., Honda, S., Tahara-Hanaoka, S., Miyamoto, A., Onodera, M., Sumida, T., Nakauchi, H., Miyoshi, H., and Shibuya, A. (2003). CD226 (DNAM-1) is involved in lymphocyte function-associated antigen 1 costimulatory signal for naive T cell differentiation and proliferation. J. Exp. Med. *198*, 1829–1839. https://doi.org/10.1084/jem.20030958.

Spees, J.L., Olson, S.D., Whitney, M.J., and Prockop, D.J. (2006). Mitochondrial transfer between cells can rescue aerobic respiration. Proc. Natl. Acad. Sci. U S A. *103*, 1283–1288. https://doi.org/10.1073/pnas.0510511103.

Spinazzi, M., Casarin, A., Pertegato, V., Salviati, L., and Angelini, C. (2012). Assessment of mitochondrial respiratory chain enzymatic activities on tissues and cultured cells. Nat. Protoc. *7*, 1235–1246. https://doi.org/10.1038/nprot.2012.058.

Stegemann, S., and Bock, R. (2009). Exchange of genetic material between cells in plant tissue grafts. Science *324*, 649–651. https://doi.org/10.1126/science.1170397.

Stewart, J.B., and Chinnery, P.F. (2015). The dynamics of mitochondrial DNA heteroplasmy: implications for human health and disease. Nat. Rev. Genet. *16*, 530–542. https://doi.org/10.1038/nrg3966.

Sun, C., Liu, X., Wang, B., Wang, Z., Liu, Y., Di, C., Si, J., Li, H., Wu, Q., Xu, D., et al. (2019). Endocytosis-mediated mitochondrial transplantation: transferring normal human astrocytic mitochondria into glioma cells rescues aerobic respiration and enhances radiosensitivity. Theranostics *9*, 3595–3607. https://doi.org/10.7150/thno.33100.

Tachibana, M., et al. (2009). Mitochondrial gene replacement in primate offspring and embryonic stem cells. Nature *461*, 367–372. https://doi.org/10.1038/nature08368.

Tachibana, M., et al. (2013). Towards germline gene therapy of inherited mitochondrial diseases. Nature *493*, 627–631. https://doi.org/10.1038/nature11647.

Tan, A.S., Baty, J.W., Dong, L.F., Bezawork-Geleta, A., Endaya, B., Goodwin, J., Bajzikova, M., Kovarova, J., Peterka, M., Yan, B., et al. (2015). Mitochondrial genome acquisition restores respiratory function and tumorigenic potential of cancer cells without mitochondrial DNA. Cell Metab. *21*, 81–94. https://doi.org/10.1016/j.cmet.2014.12.003.

Wallace, D.C. (1994). Mitochondrial DNA sequence variation in human evolution and disease. Proc. Natl. Acad. Sci. U S A *91*, 8739–8746. https://doi.org/10.1073/pnas.91.19.8739.

Wallace, D.C. (2005). A mitochondrial paradigm of metabolic and degenerative diseases, aging, and cancer: a dawn for evolutionary medicine. Annu. Rev. Genet. *39*, 359–407. https://doi.org/10.1146/annurev.genet.39.110304.095751.

Wallace, D.C. (2018). Mitochondrial genetic medicine. Nat. Genet. *50*, 1642–1649. https://doi.org/10.1038/s41588-018-0264-z.

Yamaguchi, T., Hamanaka, S., Kamiya, A., Okabe, M., Kawarai, M., Wakiyama, Y., Umino, A., Hayama, T., Sato, H., Lee, Y.S., et al. (2012). Development of an all-in-one inducible lentiviral vector for gene specific analysis of reprogramming. PLoS One *7*, e41007. https://doi.org/10.1371/journal.pone.0041007.

Zhang, John, et al. (2017). Live birth derived from oocyte spindle transfer to prevent mitochondrial disease. Reproductive BioMedicine Online *34*, 361–368. https://doi.org/10.1016/j.rbmo.2017.01.013.

STAR★METHODS

KEY RESOURCES TABLE

REAGENT or RESOURCE	SOURCE	IDENTIFIER
Antibodies		
Olig2 antibody	Sigma	#AB9610; RRID: AB_570666
Sox9 antibody	Sigma	#AB5535; RRID: AB_2239761
Iba1 antibody	FUJIFILM Wako Pure Chemical Corporation	#019-19741; RRID: AB_839504
NeuN antibody	Sigma	#MAB377; RRID: AB_2298772
Cardiac troponin T antibody	BD Biociences	#565618; RRID: AB_2739306
Chemicals, peptides, and recombinant proteins		
DNase 1	Thermo Scientific	#EN0521
KSOM media	Millipore/Sigma	MR106D
Mitomycin C	Sigma	M-4287
KO DMEM	Gibco/Thermo Fisher	10829-018
LIF	Sigma	ESG1107
FBS	Fisher	SH30070
KSR	Gibco	10828-028
Trypsin-EDTA	Gibco/Thermo Fisher	15400-054
PD0325901	Sigma	PZ0162
CHIR99021	Sigma	361571
PMSG	Fisher	NC1453635
hCG	Sigma	C1063
Dapi	Sigma	D9542
Collagenase IV	Gibco/Thermo Fisher	17104019
D-PBS	Gibco/Thermo Fisher	14190-250
Hybernate A	BrainBits	HA
Hyaluronidase	Sigma	H3506
Acidic Tyrode's solution	Sigma	#T1788
Critical commercial assays		
Arcturus Pico Pure DNA extraction Kit	Invitrogen/Thermo Fisher	KIT0103
Purogen DNA purification Kit	Qiagen	# 158908; # 158912; # 158914
PCR Platinum SuperMix High Fidelity Kit	Invitrogen/Thermo Fisher	
TAKARA LA Taq polymerase	Takara/Clontech	RR002M
Nextera XT DNA kit	illumina	# FC-131-1096; # FC-131-2004
Deposited data		
Raw mtDNA sequencing data	This paper	BioProject: PRJNA803310
Experimental models: Cell lines		
Td-Tomato NZB embryonic stem cell (ESC)	This study	
GFP-B6 mutant ESC	This study	
Experimental models: Organisms/strains		
NZB mice	Jackson Laboratories	#000684
ICR mice	Charles River	#023

(*Continued on next page*)

Continued

REAGENT or RESOURCE	SOURCE	IDENTIFIER
B6 Ubc-GFP mice	Jackson Laboratories	#004353
PolG mutator mice	Jackson Laboratories	#017341
Oligonucleotides		
Primer 5′F-GGATCCTACTCTCTACAAAC-3′	This study	B6/NZB mtDNA (Fw)
Primer 5′R- AGTGGTGGAAGGCCTCCTAG-3′	This study	B6/NZB mtDNA (Rv)
Primer 5′F- GCTGGACATCACCTCCCACA-3′	This study	Td-Tomato nDNA (Fw)
Primer 5′R- GCCGTACAGGAACAGGTGGT-3′	This study	Td-Tomato nDNA (Rv)
Probe FAM-ACGAGCGCTCCGAGGGCCGC	This study	Td-Tomato nDNA (Probe)
Primer 5′F- CCTCGTCCCCATTCTAATC TCT-3′	This study	Unique NZB mtDNA (Fw)
Primer 5′R- GTTAGGGCCTTTTCGTAGTTG TATA-3′	This study	Unique NZB mtDNA (Rv)
Probe FAM- ACACTAGTAGAACGCAAAAT	This study	Unique NZB mtDNA (Probe)
Primer 5′F- AATTTCATATGAAGTAACCATA GCTCTT-3′	This study	Unique B6 mtDNA (Fw)
Primer 5′R- CTGGCAGAAGTAATCATATG CGT-3′	This study	Unique B6 mtDNA (Rv)
Probe FAM- TGGATCCTACTCTCTACAAAC	This study	Unique B6 mtDNA (Probe)
Primer 5′F- GCCTCGTACCAACACATGATC-3′	This study	Common NZB and B6 mtDNA (Fw)
Primer 5′R- GGACTTCTAGAGGGTTAAGTG GTG-3′	This study	Common NZB and B6 mtDNA (Rv)
Probe TET- CTGACCTCCAACAGGAA	This study	Common NZB and B6 mtDNA (Probe)
Primer 5′F- GATTTTGTCGTTCTCAAACA CCA-3′	This study	Unique B6 nDNA (Fw)
Primer 5′R- TTTCTGGCTCAGCTCATGG-3′	This study	Unique B6 nDNA (Rv)
Probe FAM- CCGTGTCTTCCCAGCAGGTGT GCAGGC	This study	Unique B6 nDNA (Probe)
Primer 5′F- TGAGGGGCAGGATTTTGTC-3′	This study	Common B6 nDNA (Fw)
Primer 5′R- TGGCTTTCTGGCTCAGCTC-3′	This study	Common B6 nDNA (Rv)
Probe FAM- CCGTGTCTTCCCAGCAGGT GTGCAGGC	This study	Common B6 nDNA (Probe)
Primer 5′F-GGATCCTACTCTCTACAAAC-3′	This study	Fragment 1 mtDNA (Fw)
Primer 5′R- TAGTTTGCCGCGTTGGGTGG-3′	This study	Fragment 1 mtDNA (Rv)
Primer 5′F- CTACCCCCTTCAATCAATCT-3′	This study	Fragment 2 mtDNA (Fw)
Primer 5′R- CCGGTTTGTTTCTGCTAGGG-3′	This study	Fragment 2 mtDNA (Rv)
Software and algorithms		
Trim Galore (v0.6.3)	N/A	https://www.bioinformatics.babraham.ac.uk/projects/trim_galore/
BWA-MEM (v0.7.17)	N/A	http://bio-bwa.sourceforge.net/
Picard tools (v2.18.2)	N/A	https://broadinstitute.github.io/picard/
FreeBayes (v1.3.1)	N/A	https://github.com/freebayes/freebayes
SAMtools (v1.10)	N/A	http://www.htslib.org/
Sequencher (v4.10.1)	N/A	http://www.genecodes.com/
RStudio (v1.3.1093)	N/A	https://www.rstudio.com/products/rstudio/
R (v4.0.3)	N/A	https://cran.r-project.org/

(*Continued on next page*)

Continued

REAGENT or RESOURCE	SOURCE	IDENTIFIER
SoftMax Pro software	N/A	https://www.moleculardevices.com/products/microplate-readers/acquisition-and-analysis-software/softmax-pro-software
GraphPad Software	N/A	https://www.graphpad.com/quickcalcs/

RESOURCE AVAILABILITY

Lead contact

Further information and requests for resources and reagents should be directed to and will be fulfilled by the lead contact Shoukhrat Mitalipov (shoukhrat@gmail.com)

Materials availability

This study did not generate new unique reagents.

Data and code availability

- Sequencing data has been deposited in the Sequence Read Archive (SRA) of the NCBI and are publicly available as of the date of publication. Accession numbers are listed in the key resources table.
- This paper does not report any original code.
- Any additional information required to reanalyze the data reported in this paper is available from the lead contact upon request.

EXPERIMENTAL MODEL AND SUBJECT DETAILS

Mice strains

All animal experiments were approved by the Institutional Animal Care and Use Committee (IACUC) at Oregon Health & Science University (OHSU). All mice were maintained under specific pathogen free and controlled lighting conditions (12 hours light/dark cycles) at OHSU. Mice were housed in individually ventilated cages with HEPA filtered supply ventilation with a maximum of 5 mice per cage. Caging, bedding and accessories were sterilized prior to use. All handling of animals occurred in HEPA filtered biosafety cabinets and mice were handled with gloves. Mice were provided with Irradiated Lab Diet Pico Lab Rodent Diet (5LOD) or LabDiet Pico Mouse Diet 20 (5058). Water was supplied by chlorinated reverse osmosis (RO) water to auto-water ventilated racks. Mice were checked daily by comparative medicine staff and any concerns were immediately reported for examination by a staff veterinarian.

Females used to obtain embryos were 6-8 weeks old. Surrogated females were 8 weeks old. Males for breeding or vasectomized males were between 8 weeks to 8 months old. A total of 62 chimeric mice (25 females and 37 males) were created for this study. Chimeras were maintained up to 21 months of age.

ESC derivation

NZB morula-blastocyst stage embryos were cultured 24 hours in KSOM medium. The zona pellucida was removed with acidic Tyrode's solution (Sigma-Aldrich) and blastocysts were individually plated onto mitomycin C (Sigma-Aldrich) treated mouse embryonic fibroblast (mEF) feeder layers in ES derivation medium: KODMEM (Invitrogen) containing 1mM L-glutamine, 100 units/mL penicillin, 100 μg/mL streptomycin, 100 μM β-mercaptoethanol (Sigma), 100 μM nonessential amino acids (Invitrogen), 1,000 units/mL LIF (Millipore), 10% FBS and 10% KSR (Invitrogen). ICM outgrowth colony was collected and dispersed into single cells using 0.15% trypsin solution (Sigma-Aldrich) before replating onto fresh mEF in ES medium containing 1 μM PD0325901 (Axon) and 3 μM CHIR99021 (Axon).

To induce fluorescent marker uniformly expressed under the control of the Ubiquitin-C promoter in NZB ES cell lines, Ubc-Td-tomato coding sequence was cloned into lentiviral vector with pPACKH1 (SBI) and Purfection (SBI) (Shibuya et al., 2003; Yamaguchi et al., 2012). The presence of Ubc-Td-tomato expression was examined by fluorescence under 568 nm light and confirmed by FACS sorting purification (BD AriaII). GFP

labeled B6 ESC line carrying mtDNA mutations, were generated using PolG mutator mice and B6 Ubc-GFP mice (Jackson laboratory) as recently described (Ma et al., 2020).

METHOD DETAILS

Collection of 2-cell stage embryos and blastocysts

Six-eight weeks old NZB, ICR and B6 females were injected with 5 international units of pregnant mare's serum gonadotropin (PMSG) and human chorionic gonadotropin (hCG). Two-cell stage embryos were collected from excised oviducts 44 hours post hCG injection. Morula-blastocyst stage embryos were flushed and collected from uteri of E2.5 super-ovulated females.

Chimera generation

Chimeric mice have been created by either aggregation of cleaving embryos or injection of ESCs into cleaving host embryos. For aggregation, a pair of 4-8-cell stage ICR and NZB embryos were freed of zona pellucida, aggregated together in micro wells and cultured for 48hrs in AA-KSOM (Millipore) at 37°C and 5% CO2. Alternatively, 4–8-cell stage ICR host embryos were injected with NZB-Ubc-Td-tomato ESCs and 4–8-cell stage host NZB embryos were injected with B6-Ubc-GFP ESCs to generate chimeras. Injected embryos were cultured for 24 hrs in AA-KSOM medium (Millipore) at 37°C and 5% CO2 to blastocysts and then transferred to uteri of pseudo pregnant (E2.5 or E3.5) ICR females (recipients). Implantation sites were examined at gestation day 21.

Premixed non-chimeric controls

For each control experiment, one ICR and one NZB mice were euthanized and organs from both animals were minced together as one sample. The downstream processing and single cell collection was performed similar to chimeras.

Single cell collection

Heart, brain, intestine, spleen, kidney, liver, testis and oocyte-cumulus complex were processed to obtain a single cell suspension. Tissues were mechanically chopped with scissors. Testis, kidney, liver and spleen were then placed in PBS and filtered through a 40μm cell strainer. Red blood cells in kidney, liver and spleen were lysed using red blood cell lysing solution (0.15M NH_4Cl (Sigma), 1mM $NaHCO_3$ (Sigma) and 0.1mM EDTA (Sigma)). Remaining cell suspension was washed twice in PBS with 5% of FBS, filtered through 35μm nylon mesh, treated with DAPI, 1μg/mL (Sigma) and kept in the dark on ice until sorted. Chopped intestine and heart tissues were placed in 2mL of DMEM containing 1mg/mL collagenase IV (Gibco) and were digested for 30 minutes at 37C. Digested solution was vortex twice, 5 sec each and filtered through 40 μm strainer followed by washing twice in PBS with 5% of FBS at 1000rpm, 3 minutes. Cell pellet was resuspended in PBS with 5% FBS and kept on ice until used. Intestinal cell suspension was then filtered and treated with DAPI as described above. Brain tissue was processed following Guez-Barber paper (Guez-Barber et al., 2012). Briefly, mechanically chopped brain tissue was resuspended in Hybernate A medium (BrainBits) and cells were separated using three different diameter pipettes followed by two centrifugations through three layers of density gradient. Final pellet was resuspended in PBS with 5% FBS, treated with DAPI and kept on ice. The cell suspension was treated with 125 U/mL DNase 1 (Thermo Scientific, EN0521) for 15-60 min. Oocyte-cumulus complexes were collected from oviducts and cumulus cells were disaggregated using 1mg/mL hyaluronidase (Sigma). Cumulus cells were washed and kept in PBS with 5% FBS on ice until used. Oocytes were washed in 5 drops of KSOM media and collected immediately. Cells from every tissue but heart were FACS sorted (BD Influx). From chimeras ICR/NZB-Td-tomato, two group of cells were obtained by fluorescence under 568nm being separated by presence of Td-tomato. From chimeras NZB/B6-GFP, two group of cells were obtained by fluorescence under 499nm being separated by presence of GFP.

Cells were washed in 2 serial drops of PBS with 5% of FBS. From there cells were selected using micromanipulator on an inverted microscope. Visually healthy cells observed in 20X magnification, were collected and washed in at least 5 new drops before being collected in no more than 0.1 μL volume. The washing in serial drops decreased the chances of collecting cell-free DNA.

Single cell DNA extraction

Individual cells were transferred into a 0.2mL PCR tubes and DNA was extracted using an Arcturus Pico Pure DNA extraction kit (Applied Biosystems) following the manufacturer protocol. Bulk DNA from tissues was

extracted using a Purogen DNA purification kit (QIAGEN) according to the manufacturer's instructions. NanoDrop 2000 spectrophotometry (NanoDrop technologies) was used for DNA mass determinations.

Heteroplasmy detection by sanger

Target region was amplified using a PCR Platinum SuperMix High Fidelity Kit (Life Technologies) with primer set: 5'F-GGATCCTACTCTCTACAAAC-3' and 5'R- AGTGGTGGAAGGCCTCCTAG-3'. PCR products were purified, Sanger sequenced and analyzed by Sequencher v4.10.1 (GeneCodes). The 4 SNV analyzed were 3422 C>T, 3467 C>T, 3599 C>T and 3692A > G.

Heteroplasmy quantification by quantitative (q) PCR and amplification refractory mutation system (ARMS)-qPCR

qPCR was used to measure nDNA chimerism in bulk DNA isolated from each organ. Primers and probe were designed to target Td-Tomato (5'F- GCTGGACATCACCTCCCACA-3', 5'R- GCCGTACAGGAAC AGGTGGT-3', FAM-ACGAGCGCTCCGAGGGCCGC). ARMS-qPCR was used to measure mtDNA heteroplasmy in single cardiomyocytes as previously described (Lee et al., 2012). This qPCR method is based on quantification of less abundant mtDNA variant using discriminative and consensus assays. For the discriminative assays, primers and TaqMan probes were designed to target the unique mtDNA region for NZB mtDNA (5'F- CCTCGTCCCCATTCTAATCTCT-3', 5'R- GTTAGGGCCTTTTCGTAGTTGTATA-3', FAM- ACA CTAGTAGAACGCAAAAT), B6 mtDNA (5'F- AATTTCATATGAAGTAACCATAGCTCTT-3', 5'R- CTGGCA-GAAGTAATCATATGCGT-3', FAM- TGGATCCTACTCTCTACAAAC) and the unique nuclear DNA region for B6 nDNA (5'F- GATTTTGTCGTTCTCAAACACCA-3', 5'R- TTTCTGGCTCAGCTCATGG-3', FAM- CCG TGTCTTCCCAGCAGGTGTGCAGGC). For the non-discriminative assay, primers and TaqMAn probes were designed to target common region for mtDNA (NZB in B6 and B6 in NZB) (5'F- GCCTCGTACCAA-CACATGATC-3', 5'R- GGACTTCTAGAGGGTTAAGTGGTG-3', TET- CTGACCTCCAACAGGAA), and B6 in NZB nDNA (5'F- TGAGGGGCAGGATTTTGTC-3', 5'R- TGGCTTTCTGGCTCAGCTC-3', FAM- CCGTG TCTTCCCAGCAGGTGTGCAGGC).

Whole mtDNA sequencing

Whole mtDNA was amplified by two-fragment PCR reaction using the primers sets 5'F-GGATCC TACTCTCTACAAAC-3', 5'R- TAGTTTGCCGCGTTGGGTGG-3' and 5'F- CTACCCCCTTCAATCAATCT-3', 5'R- CCGGTTTGTTTCTGCTAGGG-3' and using TAKARA LA Taq polymerase (Takara biotechnology, Shiga, Japan). Concentration of PCR products was measured by the Qubit 2.0 Fluorometer (Invitrogen). Amplified PCR products were normalized and used for library preparation with the Nextera XT DNA kit (Illumina, San Diego, CA, USA) following manufacturer's instructions. Paired-end sequencing was performed on the Illumina MiSeq platform as 2x250 or 2x150bp at the Molecular Technologies Support Core of ONPRC (OHSU) and/or at Asan Medical Center (South Korea).

Sequencing data analysis and heteroplasmy quantification

Sequencing reads underwent adaptor trimming using Trim Galore (v0.6.3) and were mapped to the mouse mtDNA reference genome (NC_005089.1) using BWA-MEM (v0.7.17). Duplicate reads were identified and marked by Picard tools (v2.18.2). mtDNA variant frequencies were discovered via frequency-based pooled calling with FreeBayes (v1.3.1) with local left-alignment of indels and further normalized with SAMtools (v1.10). We further applied additional filters (QUAL>1, SAF>0, SAR>0) to keep only high-confident variant calls. Average variant coverage depth was 1,468X. Point heteroplasmy was assessed at 88 nucleotide positions as an alternative allele frequency divided by total site coverage, with a reporting threshold of 2% for minor sequence variant. For mean heteroplasmy calculation, maximum of 84 allele frequency values representing all 88 mtDNA variants were used. This strategy represented more accurate mean heteroplasmy assessment and was chosen due to the observation that 8 variants covered by 4 alleles (two variants per allele) always had the same allele frequency.

Mitochondrial respiratory chain enzyme assays

Respiratory chain complex I and IV activities were assayed in both ESC lines by spectrophotometric methods as describe previously (Spinazzi et al., 2012). A VersaMax microplate reader system (Molecular Devices) in combination with SoftMax Pro software was used for activity measurements and calculations. Enzyme activities were expressed as a percentage relative to rotetone inhibition in complex I and as absolute value (nmol/min/mg protein) in complex IV.

Immunostaining

Dissociated brain cells were plated on poly-D-lysine coated glass bottom dishes and allow to adhere for 1 hr. Cell then fixed for 20 mins in 4% paraformaldehyde and washed 3 times with PBS. Cell were permeabilized and blocked for 1hr using blocking buffer (1% BSA, 0.1% Triton X-100 and 1% fish skin gelatin). Cell were then incubated overnight at 4°C with antibodies specific for oligodendroglia (Olig2), astrocytes (Sox9), microglia (Iba1) and neurons (NeuN). Cardiomyocytes were labeled with cardiac troponin T (BD-565618). Nuclei were co-stained with either PI or DAPI.

Immunolabelled cells were imaged using a Nikon A1R confocal microscope using a 10X objective. Captured images were analyzed by manual counting of positively stained cells/nuclei for each cell type marker, using FIJI Cell Counter plugin. Total cell numbers were counted in a given field using nuclear staining.

QUANTIFICATION AND STATISTICAL ANALYSIS

Statistical analysis was performed in GraphPad Prism. Fisher's exact test with two tails was used for the comparison between numbers of heteroplasmic cells. Student's t-test was used for comparison of percentage of donor mtDNA, % of chimerism and mitochondrial complex activity, which was presented as mean $\pm$ SEM. Significant was set at $P<0.05$.